Ecological Modelling
February 2008, Volume 210, Issue 4, Pages 351-376
http://dx.doi.org/10.1016/j.ecolmodel.2007.08.025

Modelling the Karenia mikimotoi bloom that occurred in the western English Channel during summer 2003

Alice Vanhoutte-Brunier[a, b], Liam Fernand[c], Alain Ménesguen[a, *], Sandra Lyons[d], Francis Gohin[a] and Philippe Cugier[a]

[a]IFREMER Centre de Brest, BP 70, 29280 Plouzané, France
[b]IFREMER Centre de Boulogne-sur-mer, BP 699, 62200 Boulogne-sur-Mer, France
[c]CEFAS Lowestoft Laboratory, Pakefield Road, Lowestoft, Suffolk NR33 OHT, UK
[d]Martin Ryan Institute, National University of Ireland, Ireland

*: Corresponding author : Alain Ménesguen, email address : Alain.Menesguen@ifremer.fr

Abstract:

Observations from space and in situ from the R.V. Corystes 8/03 Cruise show that a massive Karenia mikimotoi bloom occured during summer 2003 in the western English Channel. Due to exceptional climatoligical conditions that occured in June 2003, the installation of a very strong thermocline enhanced the development of a massive bloom over 1 million cells l−1 in the Central English Channel. This paper presents the application of a mathematical model of this species, previously developed in for the Bay of Biscay, into a general 3D model of the primary production of the English Channel and southern Bight of the North Sea. Allelopathic interactions exerted by K. mikimotoi on other phytoplankton species and the role of agitation in the mortality of this species are taken into account. The model includes the dynamics of the bloom and consequently reproduces with good agreement the geographical distribution of the K. mikimotoi bloom both surface and subsurface. The model suggests that the apparent transport of the bloom towards the French coasts as inferred from the satellite observation was not due to advection but was only caused by the establishment of suitable conditions. The sensivity of the K. mikimotoi distribution to boundary conditions, initialization and the role of turbulence is discussed.

Keywords: Coupled physical-biogeochemical 3D modelling; *Karenia mikimotoi*; Primary production; SeaWiFS; Western English Channel

1 Introduction

Harmful algal blooms have occured for many centuries in many pelagic ecosystems, before the possible influence of significant human activity, however, during the last decades these events have increased in number, areal distribution and biomass (Anderson, 1997; Chrétiennot-Dinet, 1998; Riegman, 1998; Granéli, 2004). They have many forms and effects (Anderson, 1997), impressive primary production by non-toxic algae can provoke a temporary oxygen deficiency when decaying and strongly disturb the ecosystem. This primary production can often occur during a short period. A number of other species, for example *Dinophysis*, are poisonous at low concentrations. Estimates of the number of phytoplanktonic species that contain toxins varies from 60-78 (Sournia, 1995) to 100 (Granéli, 2004). The majority of these species belong to the Dinophyceae class (Sournia, 1995). Among them, the dinoflagellate *Karenia mikimotoi* is observed in all of the oceans and particularly in the coastal waters of northern Europe. This species was previously described as *Gyrodinium aureolum*, *Gymnodinium* cf. *nagasakiense* and *Gymnodinium mikimotoi*. *Karenia* G. Hansen and Moestrup is a new genus defined by Daugbjerg *et al.* (2000). It is responsible for the red to dark-brown discolouring waters when the density reaches over one million *cells* l^{-1}. Effects on marine fauna are measurable above a few million cells per litre (Gentien, 1998). The production of high rates of viscous extracellular polysaccharides can cause asphyxiation in fish, a property called "rheotoxicity" (Jenkinson and Arzul, 1998, 2001). Widespread mortality events of wild fishes and benthic invertebrates were observed along the English south coast in 1978 and off the southwest Ireland in 1976 and 1978 (review of Jones et al. 1982). The economic consequences of fish kills due to red tides can be significant, e.g. fish farms in Scottish lochs in September 1980 (review of Jones et al. 1982), 3,546 tons of caged fish were killed in Hong-Kong Bay in 1998 (Hodgkiss and Yang, 2001; Yang and Hodgkiss, 2001). In 1985, the occurence of a bloom at 800,000 *cells* l^{-1} of *K. mikimotoi* in the Bay of Brest caused a loss of 4,000,000 individuals in scalop nurseries and culture trays (Erard-Le Denn *et al.*, 2001). Along the French Atlantic coast, a mortality of 800-900 tons of the mussel *Mytilus edulis* (Gentien, 1998) and many fish in 1995 coincided with an exceptional bloom of 48 million *cells* l^{-1} (Arzul *et al.*, 1995). Exotoxin production can also affect the growth of other algae, this allelopathic effect has been demonstrated in many phytoplankton groups, for example on the diatom *Chaetoceros gracile* in the Ushant Front (Arzul *et al.*, 1993) and on a natural population of dinoflagellates (Fistarol *et al.*, 2004).

In the western English Channel, blooms of this species have often been observed in the Ushant Front (Pingree, 1975; Holligan, 1979; Holligan *et al.*, 1984; Garcia and Purdie, 1994) and in the seasonally stratified region which extends from the central western English Channel to the coast of Cornwall (Le Corre *et al.*, 1993; Rodrìguez *et al.*, 2000). These monospecific blooms can reach many millions of cells per litre and represent up to 100 $mg\ m^{-3}$ of chl-a (Holligan, 1979).

During summer 2003, spectacular sea surface chlorophyll a (SS-Chl$a$) concentrations were observed from space by ocean colour images. Observations from the *R.V. Corystes* Cruise 8/03 from 26th June to 9th July 2003 in the western English Channel highlighted that these high chlorophyll concentrations were due to a monospecific bloom of *K. mikimotoi*. The exceptional characteristic of this event is visible in Figure 1 (SS-Chl$a$ derived from SeaWiFS), while blooms are common in this area, the 2003 bloom started much earlier and reached a much greater cell

density (up to 1,000,000 *cells* l^{-1}).

A modelling study of *K. mikimotoi* blooms in the context of the Bay of Biscay was first developed by Loyer (2001) and Loyer *et al.* (2001). The goal of this work is to introduce the Loyer's *K. mikimotoi* submodel in a regional ecosystem model of the Channel and southern North Sea, in order to test the robustness of this model in another ecosystem which is hydrodynamically and hydrologically different from the Bay of Biscay. The model is also used to evaluate the importance of each process in the *Karenias*'s dynamics and the sensitivity of the model to some parameters.

2 Description of the study site

The English Channel is part of the Northwest European continental shelf, it connects the Atlantic Ocean to the North Sea (Fig. 2). Its boundaries are normally defined as the Dover Strait in the east, with the western end marked by the Isles of Scilly (UK) to Ushant (France). This system receives significant freshwater and nutrient inputs, in the east, from the river Seine (mean flow about 600 m^3 s^{-1}). However, the rivers that discharge into the western English Channel contribute very little to the overall input of nutrients compared to loadings of water masses coming from the Atlantic.

The strong tidal regime leads to a range of hydrographic features, such as the high tidal range in the region of the Normand-Breton Gulf (Fig. 2), a complicated gyre system around the Channel islands of Jersey and Guernsey (Salomon *et al.*, 1988), strong tides in the Dover straits with the residual circulation generally directed to the North Sea (Prandle *et al.*, 1993). North of the Bay of Seine, along the French coast of the eastern English Channel, a front limits a narrow strip of fresher and chl-*a* richer waters called the "coastal flow" (Quisthoudt, 1987; Brylinski *et al.*, 1991). In the Bay of Seine, high river flows induce a plume with strong horizontal and vertical gradients.

Further west with weaker tides the waters stratify, where the Ushant Tidal Front (drawn in Fig. 2) separates well mixed waters along the north-western coast of Brittany, from summer stratified shelf waters of the central English Channel (Pingree, 1975).

3 The model

During the last decades, the enhanced computer capacities allowed to build sophisticated models in terms of spatial refinement and biochemical complexity. 3D models are useful for the study of harmful algae events which are associated to local imbalance of nutrients or/and to local specific hydrodynamical structure. Ecological models are developped to study the dynamics of macroalgae (eg. *Zostera marina* in Mediterranean lagoons, Zharova *et al.*, 2001; Plus *et al.*, 2003; Pastres *et al.*, 2004; *Ulva lactuca* in the Bay of Brest, Ménesguen *et al.*, 2006) or microalgae species (eg. *Phaeocystis globosa* in the Channel and southern North Sea, Lacroix *et al.*, 2007). Some of them are coupled to models of the catchment area of the rivers that discharge in the area of interest, like lagoons (eg. the Thau lagoon, Plus *et al.*, 2006) or bays (eg. the Bay of Seine, Cugier *et al.*, 2005a). In such enclosed environments, the oxygen dynamics is investigated

because of the mortality of various aerobic organisms wich results from the oxygen deficiency and its total disappearence in the bottom layer (Plus *et al.*, 2003; Tuchkovenko and Lonin, 2003). The accumulation of detrital organic matter, as a consequence of massive algal blooms, increases the oxygen demand for biochemical oxidation.

Good reviews of regional ecosystem models of the European Shelf can be found in the papers of Moll (1998) and Allen *et al.* (2001). Real coupling studies between general circulation models and ecosystem models appeared in late 1990's with generally quite large meshes of 20 km (Skogen *et al.*, 1995; Moll, 1998). As far as the biogeochemical modelling strategy is concerned, models differ from the number of cycles taken into account (among N, P, Si, C), the number of prognostic variables and the growth's scheme chosen (Flynn, 2003). First models were of Nutrient-Phytoplankton-Zooplankton type. Trophic pathways have been expansed to microbial processes and to the benthic fauna. Actually, one of the more complex ecological model is ERSEM (Baretta *et al.*, 1995; Ebenhöh *et al.*, 1997; Baretta-Bekker *et al.*, 1998). It describes the N, P, Si and C cycles in both pelagic and benthic foodwebs. Allen *et al.* (2001)'s model of the North West European Continental Shelf ecosystem is the first that combines both high spatial refinement and high biogeochemical complexity at a so large scale. It couples the biogeochemical module of ERSEM to the POL-3DB baroclinic model (Proctor and James, 1996; Holt and James, 2001) on a 12 km grid. Recently, Lacroix *et al.* (2007) coupled the mechanistic model MIRO (Lancelot *et al.*, 2005), which in particular describes the dynamics of the mucilage forming algal species *Phaeocystis globosa*, with the high resolution 3D hydrodynamical model COHERENS applied to the Channel and Southern Bight of the North Sea (Lacroix *et al.*, 2004).

In this study, the hydrodynamical model MARS3D is directly coupled to a biogeochemical model that describes locally the evolution of the non-conservative variables in water and sediment. At the same time, the hydrosedimental model SiAM-3D (Cugier and Le Hir, 2000) computes exchanges of particulate matters at the water/sediment interface from erosion and deposition processes. The sedimental velocity of diatoms and detrital matters are assessed, at each time step, in the biogeochemical module. The diffusion of dissolved substance between the multilayered sedimental bed and the bottom layer of the water column follows the concentration gradient.

3.1 The hydrodynamical model

In the Channel, due to the strong tidal gradient and the presence of small scale features a high resolution model is required. In this work, the MARS3D provides high resolution physical 3D characteristics. It was developed by Ifremer (Lazure and Jégou, 1998; Lazure and Dumas, 2006) and is commonly used in many oceanographic regions some with coupling to higher trophic levels. It uses a finite difference scheme to solve the primitive Navier-Stokes equations under both hydrostatic and Boussinesq assumptions. The domain simulated in this study extends from the south of Brittany (47.5 $^\circ$N, 5.6 $^\circ$W) to north of the Rhine river plume (52.5 $^\circ$N, 5.0 $^\circ$W). The model is in spherical coordinates; the mean size of meshes is about 4 km by 4 km. The water column is divided into 12 layers all over the domain and the thickness of the layers follows the bathymetry (σ-coordinates). The layers in the first third of the water column are thinner in order to have a good representation of the thermo-haline stratifications.

The bathymetry is provided by the SHOM (Service Hydrographique et Océanographique de la Marine, France).

3.2 The biogeochemical model

The aim of this ecosystem model is to reproduce the dynamics of the free-living plankton with a simple biogeochemical model, similar to that previously developed for the Bay of Biscay (Loyer *et al.*, 2001; Huret *et al.*, 2007), the Bay of Seine (Ménesguen *et al.*, 1995; Guillaud *et al.*, 2000; Cugier *et al.*, 2005b) and the Channel (Hoch and Ménesguen, 1997; Ménesguen and Hoch, 1997; Hoch, 1998; Hoch and Garreau, 1998). The originality of our approach lies in the adding of a specific submodel *Karenia mikimotoi*, as previously applied in the Bay of Biscay (Loyer *et al.*, 2001).

3.2.1 State variables and common processes

The biochemical model is an extension of the NPZD model type (Nutrient-Phytoplankton-Zooplankton-Detritus). The model of the planktonic network (Figure 3) aims to simulate the fluxes between each level with only limiting elements such as nitrogen, silicon and phosphorus modelled, while carbon, the main constituent of the algal biomass, is not explicitly simulated because it is provided in non-limiting concentrations in marine systems by respiration and air-sea exchanges (Ménesguen *et al.*, 2001). Oxygen in the sediment is also modelled due to its role in the fate of phosphorus and nitrogen in the sediment.

In the model, the phytoplankton feeds on two dissolved inorganic nitrogen forms, nitrate (NO_3^-), ammonia (NH_4^+) and the dissolved orthophosphate (PO_4^{2-}). For (PO_4^{2-}) due to its high affinity with sediment particles and suspended matter in the water column, exchanges through adsorption and desorption with the particulate exchangeable phosphate pool (Pads) are handled using kinetics already described in Guillaud *et al.* (2000) and Cugier *et al.* (2005b). The last nutrient required for siliceous algae (diatoms) is silicate ($\mathsf{Si(OH)}_4$) and the two functional phytoplankton groups are simulated according to their dependence (diatoms Dia) or independence (dinoflagellates Din and nanoflagellates Nan) on silicon for growth. *Karenia mikimotoi* (Kar) can be distinguished from the general class of dinoflagellates by consideration of its own dynamics and the special processes linked to it. The food-chain is closed by zooplankton divided into two classes by size, the microzooplankton (Miz) and the mesozooplankton (Mez), and by benthic suspension feeders (Bent). The detrital matter (Ndet, Pdet and Sidet) is composed of faecal pellets and dead organisms.

Equations for the local evolution of the non-conservative variables are listed in table 1 with the equations that govern the processes listed in appendices A and B. Parameter values are reported in tables 2, 3 and 4. The parameters for the suspended particulate matters (SPM) which are primarily fine particles are given in table 5.

3.2.2 Factors controlling phytoplankton growth

The phytoplankton growth rate (μ in d^{-1}) depends of the availability of nutrients, the irradiance and the ambient temperature. The multi-nutrient interactions in phytoplankton growth is of Monod type, which is of low complexity. Temperature acts independently from the other factors on the mortality and on the growth according to an Arrhenius law with Q_{10}=2. Among the limiting factors (light, nutrients), the growth of each species is limited by the strongest limiting factor. However, high irradiance (above I_{opt}) inhibits growth of diatoms and dinoflagellates according to Steele's formula (Steele, 1962) but does not apply to all algal groups of the model. The light limiting function for pico-nanophytoplankton conforms to a Michaelis-Menten function. From the irradiance at the sea surface level (I_0), the availability of light for primary producers is a function of the depth (z) and the extinction coefficient (k). The equation for k has been verified in the bay of Biscay with SeaWiFS images (Gohin *et al.*, 2005) and is derived from a combination of chl-a (to account for self-shading) and SPM concentrations (appendix B). Chl-a is deduced from diatom, dinoflagellate, nanophytoplankton and *K. mikimotoi* concentrations assuming a group dependant N:chl-a. It is well known that some dinoflagellates, by the release of exotoxins, can affect the growth of their potential competitors. This allelopathic effect is exerted by *Karenia* on many sympatric species (Gentien, 1998; Hansen *et al.*, 2003; Kubanek and Hicks, 2005). Growth inhibition has been reported for diatoms (Arzul *et al.*, 1993) and for dinoflagellates (Fistarol *et al.*, 2004). Exotoxin production also induces autoinhibition (Gentien, 1998; Kubanek and Hicks, 2005) and is thus important in the termination of the bloom (see *Karenia mikimotoi* submodel, §3.2.3). Thus, adding to the Loyer (2001)'s model, this property is taken into account. A positive correlation between the density of *K. mikimotoi* and its repression of the growth of the diatom *Chaetoceros gracile* was observed in the Ushant front system (Arzul *et al.*, 1993) above a threshold *K. mikimotoi* concentration of between 7,000 and 10,000 *cells* l^{-1}. The growth attenuation rate (r_{all} in %) fitted by Arzul *et al.* (1993) is :

$$r_{all} = 11.05 \times log(\mathsf{Kar}) - 33.06 \tag{1}$$

where Kar is the concentration of *Karenia mikimotoi* in *cells* l^{-1}. Although Kubanek and Hicks (2005) showed that *K. brevis* uses species-specific allelopathic strategies, for simplicity the above equation has been applied to all phytplanktonic functional groups.

The omnivorous mesozooplankton feeds on the diatoms, dinoflagellates and microzooplankton, with the microzooplankton eating detrital matter and nanoflagellates with each class of zooplankton having its own preferential consumption behaviour (see table 3). The ingestion of the microzooplankton obeys a Michaelis-Menten equation (Hoch, 1998), whereas the capture rate of mesozooplankton follows the Ivlev's equation (Hoch, 1998). The mortality of the mesozooplankton (m_{Mez}) is a second order process linked to the concentration of Mez.
Phytoplankton and detritus can be ingested by benthic suspension feeders (Bent) located in the surface sediment. The description of the benthos dynamics is a compromise between (1) a complex system of suspension feeders as used in the benthic submodel of the Bay of Brest (Le Pape and Ménesguen, 1997; Le Pape *et al.*, 1999) and (2) a rough grazing pressure used by Savina (2004) to control the primary production in an ecosystem box model of the Channel (appendix A). The ingestion rate is higher during summer due to the use of a sinusoidal function to describe the seasonal time-course of maximum filtration. The grazing pressure and the release of matter by the benthos are only exerted on the bottom layer of the water column (layer number 1, of thickness equal to $z_{(l=1)}$).
Nutrients are regenerated by the remineralization of the detrital matters. The rate at which

diatoms sink (w^{Dia}) is linked to the nutritive limitation (f_{Nlim}) described in appendix B while the sedimentation velocity of detrital matter (w^{Det}) takes into account its origin, either phytoplanktonic or zooplanktonic. Each type of detrital matters has it's own sinking rate (w^{Det}_{Phy} and w^{Det}_{Zoo}).
All the variables involved in the nitrogen cycle are expressed in $\mu mol\ l^{-1}\ N$, except zooplankton groups ($\mu g\ l^{-1}\ dry\ wt$) and benthic fauna ($g\ m^{-2}\ C$).

3.2.3 Karenia mikimotoi submodel

The processes involved in the local evolution of *K. mikimotoi* (Kar, in $cells\ l^{-1}$) are given by (Loyer, 2001; Loyer *et al.*, 2001).

$$\frac{d\mathsf{Kar}}{dt} = \mu_{Kar} \times \mathsf{Kar} - m_{Kar} \times \mathsf{Kar}^2 \tag{2}$$

Karenia mikimotoi is extremely sensitive to agitation, Gentien (1998) observed that in cultures, the growth is optimal when the turbulence is very limited. Moreover, Gentien (1998) showed that turbulence increases the sensivity of *K. mikimotoi* to its own exotoxins. Turbulence increases the encounter rate and thus, the mortality rate. The term Kar^2 of the above equation is proportional to the encounter rate. However, *K. mikimotoi* cells secrete some mucus which leads to the aggregation of cells. The probability for cells to stay "attached" after collision and to increase the autotoxicity is expressed by the parameter α (non-dimensional) which is thermo-dependant (Jenkinson and Arzul, 1999). Thus, α evolves following an exponential function between 15 °C and 20 °C; below 15 °C, α=0.05 and above 20 °C, α=1 (Loyer *et al.*, 2001).
The mortality rate formulation integrates the shear stress (γ, in s^{-1}) resulting from the energy dissipation. According to Moum and Lueck (1985) :

$$\gamma = \sqrt{\frac{\epsilon}{7.5\ \nu}} \tag{3}$$

where ν is the kinematic viscosity. ϵ is the energy dissipation rate, which is fully computed from the turbulent kinetic energy by the MARS3D model.
Following these considerations, the mortality rate (in d^{-1}) equation is :

$$m_{Kar} = \gamma \times \alpha \times mc_{Kar} \tag{4}$$

with mc_{Kar}, the nominal mortality rate ($(cells\ l^{-1})^{-1}$).
The growth is dependent on the temperature (μ^{Kar}_T), the available light (f^{Kar}_{lum}) and nutrients (f^{Kar}_N and f^{Kar}_P) :

$$\mu_{Kar} = min(f^{Kar}_{lum}, f^{Kar}_N, f^{Kar}_P) \times \mu^{Kar}_T \tag{5}$$

The light limiting function is of Michaelis-Menten type, with a half-saturation constant (K^{Kar}_I) determined in laboratory by Loyer (2001) : $f^{Kar}_{lum} = I_z/(I_z + K^{Kar}_I)$. The value of K^{Kar}_I corresponds to an adaptation of cells to low irradiances as shown by Garcia and Purdie (1992). The nutrient limitations are assessed as for other phytoplanktonic species by a Michaelis-Menten equation. The half-saturation constant for ammonia was calibrated by Loyer *et al.* (2001) highlighting the ability of *K. mikimotoi* to grow at low mineral nitrogen concentrations (K^{Kar}_{NH4}=0.01 $\mu mol\ l^{-1}$) and to thrive mainly on ammonia ($K^{Kar}_{NH4} << K^{Kar}_{NO3}$).
Unlike the other phytoplanktonic classes, the growth of *K. mikimotoi* is directly linked to the

temperature by a polynomial function (μ_T^{Kar}). The rewiew by Loyer *et al.* (2001), gives the optimal temperature range for growth to be 14 °C-20 °C with maximum value of the growth rate to be 1.2 d^{-1} (Yamaguchi and Honjo, 1989). In this model, the growth is optimal (0.75 d^{-1}) at 15 °C and equal to 0.05 d^{-1} below 13 °C and above 23 °C. Grazing is generally an important factor on the control of the planktonic primary producers, however this not nessecarily true for *Karenia*. Rodrìguez *et al.* (2000) report consumation by *Noctiluca scintillans*, while Bjoernsen and Nielsen (1991) observed the avoidance by microzooplankton of subsurface waters dominated by *K. mikimotoi*. Birrien *et al.* (1991) noted the absence of zooplankton during a *K. mikimotoi* bloom in the Iroise Sea. It is not well established if the *K. mikimotoi* bloom area is avoided by the zooplankton or if *K. mikimotoi* is lethal for its potential predators (Gentien, 1998). As the grazing by copepods is probably low (Gentien, 1998), and perhaps nill, no top-down control is exerted on the *K. mikimotoi* population.
The conversion of the cell density of *Karenia mikimotoi* into chl-*a* concentration is done with a ratio ($r_{cell:chl}^{Kar}$) calculated with data from the Corystes cruise. Only samples with $\mathsf{Kar} > 100{,}000$ *cells* l^{-1} are kept as being nearly monospecific. $r_{cell:chl}^{Kar}$=53,000 ± 31,000 *cells* $(\mu g\, chl)^{-1}$ (n=45). Parameter values are displayed in table 3.

3.3 Initialization, forcings and boundary conditions

The transit time through the Western English Channel is typically a few months. Thus, after one year of spin-up, the initial conditions do not significantly influence the simulation. The 1 st of January concentration of diatoms is imposed following SeaWiFS-derived chl-*a* and *K. mikimotoi* is initialized as 500 *cells* l^{-1} over the domain.

A mean flow threshold of 5 $m^3 s^{-1}$ has been fixed for the selection of rivers shown on figure 2. Data was provided by the Cellule Anti-Pollution de la Seine, the Regional Agencies of the Environnement (DIREN) of Bretagne, Basse-Normandie, Nord-Pas de Calais and the Water Agencies of Loire-Bretagne, Seine-Normandie and Artois-Picardie. Data for English rivers cames from UK Environment Agency (South, South West and Thames Regions) and flow data from the National River Flow Archive of UK (NRFA). The inputs of the Rhine, Meuse and Sheldt came from the Institute for Inland Water Management and Waste Water treatment and the Rhine and Scheldt International Commissions.

The meteorological model ARPEGE (Météo-France) provided fields of air temperature, air moisture, atmospheric pressure and wind with a 0.5 ° spatial and 6 hours temporal resolution respectively. The hourly sea solar irradiance (SSI) data came from a treatment of the satellite METEOSAT-7 sensor data (Brisson *et al.*, 1994, 1996). Daily averages of the cloud cover at the Cap de La Hève meteorological station were provided by Meteo-France and were considered spatially homogeneous over the model's domain.

The free-surface elevation and currents at the open boundaries of the 3D model are off-line provided by a 2D barotropic model of greater geographic extent which covers the north-western European Shelf (from 40 °N to 65 °N and from 20 °W to 15 °W). Monthly climatologies of nutrient concentrations, salinity and temperature at the northern boundary are deduced from ICES data (`http://www.ices.dk/datacentre/data_intro.asp`). This boundary is divided into four sections to replicate the coastal-offshore gradient. Strong vertical gradients occur at

the western limit due to seasonal stratification, thus different bottom and surface values are imposed on both sides of the thermocline level computed by the model, in a similar manner to Ménesguen and Hoch (1997). The salinity is provided by a 3D model of the Bay of Biscay shelf (Huret *et al.*, 2007) and temperature is relaxed to the climatology of Reynaud *et al.* (1998) with a time lag of 13 days.

At the end of winter light availabity is the limiting factor in the growth of phytoplankton. At that period of the year, the light in the water column is governed primarily by mineral SPM whose modelling is difficult as its concentration results from the effect of sucessive strong winter storms. For that reason, we have forced the offshore SPM of our model by using monthly mineral SPM maps derived from SeaWiFS (Gohin *et al.*, 2005). This algorithm calibrated with *in situ* data deduces the non-living SPM concentration from the total SPM. From the sea surface SeaWiFS SPM data (SPM_{sat}), the computed SPM concentration (SPM_c) in the water column (depth z) is corrected by an exponential law as in Huret *et al.* (2007). This relationship is adapted in order to take into account a linear gradient effect of salinity :

$$SPM(z) = SPM_c(z) + (SPM_{sat} - SPM_c(z)) \times exp^{-\alpha \times z} \times max\Big(0; \frac{S - S_{th}}{S_{max} - S_{th}}\Big) \qquad (6)$$

with $\alpha = 0.03$, $S_{th} = 30.0$ p.s.u. and $S_{max} = 35.6$ p.s.u.. In regions of fresh water influence (defined by a salinity threshold value S_{th}=30.0 p.s.u.), the turbidity is fully described by SiAM-3D. Due to the high presence of cloud cover in the Channel, daily satellites scenes were not available, so monthly composites of the sea surface mineral SPM were constructed from SeaWiFS-derived "Ocean color" data and were interpolated to daily values to force the model.

4 Validation data

A large data set was available for the validation of the model. The stations used are displayed in Figure 2. The CEFAS research vessel Corystes (Cruise 8/03) provides an extensive source of validation with numerous CTD profiles, surface samplings and scanfish sections collected during fromthe 26 th June - 9 th July. Samples for phytoplankton analysis were taken from discrete depths at each CTD station by preserving 55 ml sub-samples withdrawn from the CTD rosette sampling bottles, in acidified Lugol's Iodine. Samples were kept cool and in the dark until analysis. Cell densities were estimated after sedimentation using the technique outlined in Raine *et al.* (1990). Cells that conformed to the description outlined in Ottoway *et al.* (1979) were scored as *Karenia mikimotoi.*

The "ocean colour" sea surface information was processed from SeaWiFS (Sea-viewing Wide Field-of-view Sensor) satellite data by an empirical specific algorithm (Gohin *et al.*, 2002, 2005). SS-Chl$a$ concentrations estimates within the bloom were above 20 $\mu g\ l^{-1}$ in the central English Channel and up to 70 $\mu g\ l^{-1}$ locally during the Corystes 08/03 Cruise. The bloom had dimensions of the order 60×30 nautical miles. According to the SeaWiFS images, the *K. mikimotoi* bloom appeared in the central western English Channel at the end of June and reached the French coast of Brittany by the beginning of August. The French Phytoplankton and Phycotoxin Monitoring Network (REPHY) counted 405,000 *K. mikimotoi cells* l^{-1} in the Saint-Brieuc

Bay on the 15th of August 2003 and the mortality of many wild fish species was observed.

The validation data set is completed with field data from regular survey networks. The Station ROS (48°46'40"N 3°56'15"W, 60 m depth) is situated off Roscoff and is part of the SOMLIT network (French national network of Marine Stations). The Station CHA (Chausey Island, 48°52.71'N 1°46.08'W, 11.5 m depth) is managed by the "Réseau Hydrologique Littoral Normand" network. E1 is a long-term time series observatory of the JGOFS program is located 20 miles off Plymouth (50°02'N 4°22'W, 55 m depth).

5 Results

The performance of the model was statistically evaluated by linear regressions between observed versus computed data. For each parameter, the slope (a) and the ordinate at origin (b) of the regression are indicated. The outputs are saved every 4 days at midday.

5.1 Seasonal stratification

Figure 5 gives the SST provided by the AVHRR at mid-July 2003 (Fig. 5a) and the difference of the monthly average of SST given by the AVHRR and the circulation model for July 2003. A mass of warmer surface water appears isolated in the central western English Channel and is limited to the south by the Ushant Front. Here, the SST reached 20.1°C on the 13th July 2003, whereas during the same period the SST along the north-western coast of Brittany was approximately 15.5°C. The model accurately reproduces these satelite - observed patterns. For two stations located in the contrasting water masses (E1 for the warmer and ROS for the cooler), computed and measured water temperature at the sea surface and bottom are displayed in Figure 4. The seasonal course of the surface-bottom temperature difference ($\Delta\Theta_{s-b}$) is also very different for these two stations. At Station E1, waters were mixed until April 2003. A smooth stratification appeared during spring, reaching a maximum measurement of approximatively $\Delta\Theta_{s-b}$ of 5.7°C on the 3rd August. This sharp two-layer structure, previously observed in the western English Channel during summer (e.g. Sharples *et al.*, 2001), is also accurately reproduced by the model (Fig. 6). The model output shows a strong thermocline at 15-20 meter, which is consitent with observations from a section perpendicular to the cornish coast. (Fig. 6b). In contrast vertically mixed waters with a maximal $\Delta\Theta_{s-b}$ of only 0.95°C (31st August (Fig. 4) exist in the coastal strip off Roscoff. The figures 4b and 5b show that the model overestimates the temperature in the coastal mixed strip by about 2°C during summer.

5.2 Spatial and temporal distribution of chlorophyll a and nutrients in 2003

In order to have an overview of the accuracy of the computed chl-a distribution, the simulated SS-Chl$a$ is compared to SeaWiFS-derived SS-Chl$a$ by using monthly averages and composites respectively (Fig. 7). These comparisons show a satisfactory agreement from March to

May 2003, especially for the onset of the spring bloom in the eastern English Channel and the southern Bight of the North Sea. High chl-a concentrations (>10 $\mu g\, l^{-1}$), exist along the coastal strip which extends from the Seine river mouth to the Dover Strait (Brylinski *et al.*, 1991) and northwards to the Rhine river mouth whereas the southern English coast and the western English Channel experianced a lower spring bloom. The SS-Chl$a$ computed north off the Bay of Somme is lower than in the corresponding SeaWiFS composit for the three spring months presented, while in the western English Channel, the computed SS-Chl$a$ is higher than the mean SeaWiFS-derived SS-Chl$a$ during May (2.5-3.0 $\mu g\, l^{-1}$ and <1.0 $\mu g\, l^{-1}$ respectively).

The ability of the model to replicate the seasonal cycle of nutrients and chl-a for the 3 stations where extensive temporal data exists is shown in Figure 8. Historical data of nitrate and phosphate (Jordan and Joint, 1998) are used as a climatology for Station E1, the other field data were collected in 2003. The chlorophyll maximum is relatively well reproduced for these three stations both temporally and in magnitude. At Station E1, the simulated chl-a maximum (4.5 $\mu g\, l^{-1}$) occurs in May, while at Station CHA in the mixed region the maximum occurs in April. Dissolved nutrients are sharply depleted after the spring bloom all over the Channel, except in the Bay of Seine, where the nutrient inputs are still supplied in summer. Thus, phytoplankton groups which have high nutrient half-saturation constants become nutrient limited (e.g. diatoms).

The seasonal cycle of the principal nutrients is well simulated except in the summer months in the coastal station where riverine sources from northern Brittany, not taken into account due to their low mean flow, have a strong local influence. The increase in ammonnia concentration at station ROS post spring bloom is due to the regeneration of detrital nitrogen and excretion from primary consumers. Subsequent to the spring bloom, the nutrient concentration for all three sites increases similarly in both the model outputs and the data. As a results of this, a smaller diatom bloom is induced during Autumn, which is consistent with previous observations (Rodrìguez *et al.*, 2000) and modelling results (Ménesguen and Hoch, 1997; Anderson and Williams, 1998; Hoch, 1998).

5.3 The 2003 Karenia mikimotoi's bloom

The figure 9 shows the computed time-depth sequence of temperature, diatoms and *Karenia mikimotoi* at Station 275. Phytoplankton counts at the sea surface revealed that the bloom was monospecific during the Corystes Cruise 8/03. Figure 10 displays the depth-maximum concentration of *K. mikimotoi* sampled during the Corystes Cruise 8/03 superimposed on the depth-maximum computed on the 12th July 2003. The model quite strongly underestimates the maximum concentration. While the *in situ* data indicates that the *K. mikimotoi* bloom reached in excess of 1,000,000 *cells* l^{-1} (1,370,800 *cells* l^{-1}, sea surface level at Station 275), the model only provides a maximum concentration of 300'000 *cells* l^{-1}. The computed *K. mikimotoi* cell density at Station 275 during 2003 is shown in Figure 9 with the diatom concentration and the temperature time-depth variation.

Massive concentrations were frequently encountered at the sea surface in the central Channel

(e.g. Station 275), while the cells seemed more abundant at the subsurface in the western region (e.g. Station 90, 1,171,100 *cells* l^{-1} at 19 m depth). If we refer to a W-E cross-section of the western English Channel (Fig. 2), the model simulates a spatially homogeneous *K. mikimotoi* maximum at 15-20 m depth (Fig. 11a) and cell densities of 75,000 *cells* l^{-1} at the sea surface. This inability of the model to reproduce high concentrations above the pycnocline is also displayed along the vertical profiles of three Corystes stations (Fig. 12). Nevertheless for 2 out of 3 stations, the subsurface concentrations provided by the model are close to observations.

6 Discussion

6.1 Global characteristics of the model

Compared to other recents ecosystem models developped in this area, ECO-MARS3D appears as a compromise between biogeochemical and hydrodynamical complexity. The phytoplanktonic compartment is described by three functionnal groups and one dinoflagellate species. Some marine ecosystem models still simulate one aggregated state variable for phytoplankton (e.g. Tuchkovenko and Lonin, 2003). The top-down control is also quite finely represented with two class of size of zooplankton. According to the meta-analysis of the 153 aquatic biogeochemical models of Arhonditsis and Brett (2004), this 16 state variables model has an intermediate level of complexity.

The model underestimates the spring phytoplankton bloom in the eastern English Channel, particularly between the mouth of the Seine river and the Dover Strait. Even if it is not our principal area of interest, many assumptions can be discussed. This area is dominated every spring by the Prymnesiophyte *Phaeocystis globosa* (Lancelot, 1995; Lefebvre and Libert, 2003), thus our model cannot reproduce these observed high chl-a concentrations. Another ecological model including a *Phaeocystis glogosa* module shows similar under-estimations of the chlorophyll-a computation (Lacroix *et al.*, 2007) in this coastal area, without one being able to say if it implies that the causes are identical into our two models. The comparison of the SS-Chl$a$ situations show that the computed coastal productive area is probably too large. The offshore dispersion of phytoplankton cells could be explained by a too diffusive advection scheme which leads to a drop of the spring peaks of phytoplankton.
In the mixed coastal strip bordering the North Brittany coast (station ROS), the computed bloom starts too early at station ROS. This is perhaps due to an insufficient grazing pressure exerted by the benthic fauna. The actual empiric feeding formula concentrates the benthos grazing pressure in summer and does not take into account any influence of the bottom current velocity. This may have a significant effect in mixed area where the suspension feeders can delay the beginning of the bloom.

Such other regional ecosystem models reproduce more or less accurately the spatial and temporal variability of chl-a concentrations. Arhonditsis and Brett (2004) assess that the simulation of the biological planktonic components is less satisfying than physical/chemical variables. Complex ecosystem models, like NEMURO model applied to the North-West Pacific Ocean (Hashioka and Yamanaka, 2007), ERSEM or MIRO use fixed sets of parameters tuned in some limits

indicated by the literature, it is often the weakest point in modelling (Jørgensen, 1999). One way to improve the parameterization of model values is data assimilisation. Applications to 3D biogeochemical models are quite limited (Arhonditsis and Brett, 2004). For the model of the Gulf of Biscay, Huret *et al.* (2007) used optimization routines that assimilate the SSChl-a deduced from ocean color data during a three weeks spring period. Even if the simulation of the spring bloom is significantly improved, it would be probably necessary to perform the optimization of the whole set of parameters at different periods. A new generation of aquatic models carries out simulations using time-varying parameters or goal functions that determine the self-organizing response of ecosystems to perturbation (Jørgensen, 1999; Arhonditsis and Brett, 2004). Such structural models are able to account for the change in the species composition as well as for the ability of species to adapt to the prevailing conditions (Jørgensen, 1999). Adaptation processes are parsimoniously used in regional ecosystem models. The ERSEM model considers an adaptation mechanism for phytoplankton to light conditions with an adaptation time of 4 days (Kholmeier and Ebenhöh, 2007). But the research on photoacclimatation processes in adimensionnal systems is much more advanced. It requires the modelling of varying intracellular ratios (N:C and Chl:C, Smith and Yamanaka, 1996). Our model does not include such complex processes than structural models do. But the focus on the parameters and equations which govers the dynamics of *Karenia mikimotoi*, one species among the dinoflagellate functionnal groups, follows a common aim, i.e. the assessment of physical and chemical conditions which control the development of one temporarly dominating microalgal species.

6.2 Controlling factors in the dynamics of Karenia mikimotoi

This study benefits of the the occurence of an exceptionnal bloom of *Karenia mikimotoi* during the Corystes 8/03 cruise. The off-shore validation of the *K. mikimotoi* submodel is more advanced than for it's first application in the Bay of Biscay Loyer (2001).

It is remarkable that from a spatial homogeneous initialization of 500 *cells* l^{-1} *K. mikimotoi* only survives in the western English Channel. Mathematical models allow to quantify the relative importance of physico-chemical factors into the phytoplankton's dynamics. The following discussion centres on why the western English Channel is the only favourable place for *K. mikimotoi*'s development.

6.2.1 Growth and mortality

The development of the bloom at the subsurface is due to favourable conditions of light, temperature, turbulence and nutrients. Modelling offers the possibility to quantify the importance of each physico-chemical factors in the development of the *Karenia* bloom (analyzed in Figure 13 for station 70). The growth limiting factors were calculated for light and each nutrient (Fig. 13a), they range from 0 (total limitation) to 1 (no limitation). Under 15 m depth, the nutritive conditions are non-limitig (f_N and f_P effects above 0.8). As previously observed by Holligan (1979), the upward mixing of nutrient-rich bottom water provides unlimited nutrient conditions for *K. mikimotoi* development at the floor of the seasonal thermocline. The subsurface bloom uses the diapycnal source of nitrogen and appears at the nitracline level (Morin *et al.*, 1989; Birrien *et al.*, 1991). As *K. mikimotoi* does not suffer from photo inhibition, favourable

light is encountered from the sea surface to 20 m depth. The maximal growth rate of 0.4 d^{-1} occurred at 20 m, where the balance of light penetration with depth against the depletion of nutrients to the surface was at an optimum for growth. These observations contribute to the idea (e.g. Smayda, 2002) that stratification primarily controls the population dynamics through interactions with the vertical irradiance and nutrient gradients. Dinoflagellates are generally the dominant photosynthetic organisms after the spring diatom outburst (eg. Holligan et al., 1979). *K. mikimotoi* represents more that 50 % of the computed sea surface phytoplanktonic nitrogen biomass in mid-July at station E1, and reached a maximum of 80 % by mid-August. *Karenia* never dominates the phytoplanktonic community at the two mixed stations.

As suggested by Le Corre *et al.* (1993), the phenomenon of the *K. mikimotoi* bloom in the fronts and offshore stratified areas differs from that in coastal waters and estuaries. In the regions of freshwater influence, the nitrogen provided for the *K. mikimotoi* bloom is generally allochthonous, derived either as dissolved inorganic (Jones *et al.*, 1982; Blasco *et al.*, 1996) or remineralized biodegradable organic nitrogen (Prakash, 1987) brought into the system in spring by the less saline waters.

Vertical profiles of the stickiness factor α and the shear stress γ are presented in Figure 13b. The shear stress γ is higher in the upper and bottom layers due to wind stress and bottom current friction respectively. The stickiness coefficient is only modulated by temperature and thus, its mean spatial distribution at the sea surface during July (Fig. 14a) quite accurately follows the SST distribution displayed in Figure 5. In a vertical profile, the mortality sharply increases above the thermocline due to the stickiness factor increasing with temperature. The role of the stickiness factor α was investigated by a sensitivity simulation using a fixed low value of α. Results are shown (Fig. 14b, left) with a corresponding depth-maximum *K. mikimotoi* reached on the 12th July with a slightly greater than the concentration reached in the reference run. The time series at station 275 (Fig. 14b, right) shows higher concentrations in July (days 180-210) at both thermocline and surface levels, when compared to the corresponding nominal situation (Fig. 9c). Therefore, without any temperature effect on mortality, the *K. mikimotoi* computed bloom is more impressive in July compared to observations. Evidence to support the relevance of this parameters comes from a second R.V. Corystes cruise from the 14th to the 27th August 2003 (results not shown) in the same area where no *K. mikimotoi* were observed. As α enhances *K. mikimotoi*'s autotoxicity property, it plays a key-role in the termination of the bloom.

Figure 15a displays the mean γ value at the sea surface.the shear stress γ is higher in the eastern English Channel Concentrations are lower (<70,000 *cells* l^{-1}) in the western English Channel when compared to the standard output (Fig. 10). Even with quite a low fixed γ value, it denotes the impact of turbulence on the start of the bloom. Interestingly in contrast with the standard run, concentrations above 25,000 *cells* l^{-1} are predicted in the eastern English Channel. The term γ in the mortality rate is of primary importance for the simulation of the spatial distribution of *K. mikimotoi*.it is the turbulent conditions that control the survival of cells transported eastwards by the residual circulation.

The accurate replication of temperature is important because it effects both the growth of *Karenia dynamics* (μ_T^{Kar}), and the mortality rate (through α). The model overestimates the SST by about 2-2.5 $^\circ$C in the mixed coastal strip delimited by the Ushant front (Figs. 5b and 4b), leading to overestimation in of growth in this area, due to the higher temperature and

reduced mixing. There is a balancing effect of increased stickiness values, increasing mortality, but α still remains quite low (< 0.4) in comparison with offshore sea surface values. This results in a slight overestimation of the *K. mikimotoi* cell concentration along the coasts of North Brittany. Similarly the model predicts *Karenia* inshore along the Cornish coast, where the model underestimates the local turbulence, possibly in the due to wave mixing in the near coastal region.

The absolute magnitude of the bloom is underestimated, as has been noted before in the Bay of Biscay (Loyer, 2001). Several behavioural mechanisms are not described in the model, in particular, the ability of *K. mikimotoi* cells to migrate vertically in relation to a nutrient tropism. This strategy of vertical depth-keeping (Smayda, 2002) is made possible by means of a swimming behaviour. *K. mikimotoi* cells can migrate vertically at approximatively 230 $\mu m\ s^{-1}$ (Throndsen, 1979). Many other assumptions can also be noted; this model considers that *Karenia mikimotoi* is autotrophic, but many studies report an assimilation of organic substances by this species (Yamaguchi and Itakura, 1999; Purina *et al.*, 2004). The ecosystem model parameterizes the microbial loop action, thus the dissolved organic pool is not described and the hypothetized mixotrophic behaviour cannot be studied. In addition, *K. mikimotoi* is able to store a large quantity of phosphorus during nutrient-replete conditions (Yamaguchi, 1994), and appears to make dark uptake of nitrate under N-limiting conditions (Dixon and Holligan, 1989). These processes all contribute to sustain *K. mikimotoi* growth.

6.2.2 Allelopathy

In our model, *Karenia mikimotoi* inhibits the growth of other phytoplankters (eq. 1). The effect begins once a sufficiently high cell concentration has been reached. It is diffucult to transpose studies reported among other HAB species, however Solé *et al.* (2005) demonstrated a such threshold effect with a simple Lotka-Volterra model calibrated with laboratory experiments and with the simulation of the *Chrysocromulina polypepsis* bloom of 1998 with the ERSEM ecosystem model.

In order to assess the importance of allelopathy in the inter-specific competition, a simulation was carried out without any inhibitory effect ($r_{all} = 1$).The depth-maximum *K. mikimotoi* concentration and the relative abundance of phytoplankton groups are displayed in Figure 16. Without an inhibitory effect, the maximum *K. mikimotoi* concentration computed at Station 275 drops from 200,000 *cells* l^{-1} to 100,000 *cells* l^{-1}. In the standard run, *K. mikimotoi* represents 60% of the total phytoplanctonic nitrogen at the end of July (Fig. 8), whereas, without the inhibitory effect, it only reaches 40 % of the N biomass (Fig. 16b).

In addition, the autumnal bloom is stronger when the inhibitory effect is removed (3.5 v.s. 1.5 $\mu g\, l^{-1}$). It demonstrates that, although the diatoms are no longer nutrient-limited, the *K. mikimotoi* exotoxins still inhibit diatom growth. However, observational evidence suggests that *K. mikimotoi* does not usually dominate the planktonic system in autumn (Rodrìguez *et al.*, 2000). It is therefore likely that the modelled termination of the bloom is certainly not abrupt enough. As the collapse of the bloom is essentially due to nutrient exhaustion (Partensky and Sournia, 1986; Morin *et al.*, 1989; Birrien *et al.*, 1991), in this instance as the magnitude of the bloom is underestimated nutrient depletion takes longer to occur. A secondary effect of the underestimation of *K. mikimotoi*'s density by the model is that the importance of self-shading

on the blooms disappearance is thus also underestimated. Additionally, other factors can affect weakened cells and thus accelerate the bloom termination, viruses are able to repress *Karenia mikimotoi* growth (Onji *et al.*, 2003) and bacteria can have an algicidal action (Yoshinaga *et al.*, 1995; Lovejoy *et al.*, 1998).

According to our assumptions (c.f. §3.2.3), *K. mikimotoï* is not grazed by zooplankton. Mukhopadhyay and Bhattacharyya (2006) investigated the role of zooplankton grazing in a theoretical NPZ system. The single phytoplanktonic compartment produces inhibitoring substances for the zooplankton. The toxication process is modelized through the grazing function of type IV due to prey toxicity. The repulsive effect exerted by the phytoplankton is incorporated through a term of zooplankton positive cross-diffusion. According to the authors, the grazing pressure could play a significant role in controlling the bloom episode for specific values of parameters. But the grazing would be a sink term in the *K. mikimotoï* equation. Since the model actually under-estimates *Karenia* cells densites, this potential lacking process is probably not a major key for the understand of the model performances.

6.2.3 Role of advection

According to SeaWiFS images, the *K. mikimotoi* bloom originally located in the central western English Channel, seemed to have a trajectory directed towards the French coast. Similar events have been persistently observed elsewhere. Raine *et al.* (1993) suggested that the red tide observed off the south-west Irish coast during the summer 1991 had been advected towards the coast from the shelf. A special run was undertaken to test the role of advection in the propagation of the bloom. A passive tracer patch of concentration 100 was initialized on the 23rd July in the central western Channel, the spill moved northwards and never reached the coasts the French coast Figure 17. The visible displacement observed from satellite is most likely due not to mass transport but to the presence of favorable conditions in successive spots closer to the coast.

6.3 Inoculum and overwintering of Karenia's cells

In contrast to other dinoflagellate species (Persson, 2000; Morquecho and Lechuga-Devéze, 2003), vegetative cells of *K. mikimotoi* are capable of overwintering (Yamaguchi, 1994; Gentien, 1998) and may not form cysts. Indeed, blooms of this eurytherm species have been reported to occur at temperatures as low as 4 $^{\circ}$C (Blasco *et al.*, 1996). A number of low winter concentrations (5-10 *cells* l^{-1}) have been observed in the Bay of Brest and it is hypothetized that the population originates from southern Brittany (Gentien, 1998). These low winter concentrations would act as the seed population for later blooms when environmental conditions are favourable.

Hydrological conditions at the entrance of the English Channel were investigated thanks to a ship of opportunity operating year-round between Plymouth (UK) and Bilbao (Spain) by Kelly-Gerreyn *et al.* (2004, 2005). Field data from 2002 to 2004 highlighted the fact that the discharge from major rivers of the Bay of Biscay (Loire, Gironde) was higher in 2003 than in 2002 and that favourable winds enhanced an unusual intrusion of lower salinity waters in

2003 (mean=34.93 p.s.u., equal in 2002 to 35.02 p.s.u.) off the North French Atlantic coast in late winter. It was hypothesized that this favoured the spectacular bloom of *K. mikimotoi* through increased buoyancy in the upper water column. If true then it demonstrates importance of good boundary conditions. In this model the salinity boundary condition is provided by a model of the Bay of Biscay (Huret *et al.*, 2007). This model is itself strongly influenced at its northern limit by the Reynaud's climatology (Reynaud *et al.*, 1998) and thus does not provide an acute enough interannual variability of hydrological conditions. It is doubtful if this model has sufficient information on salinity to adequately investigate the role of buoyancy on the success of *K. mikimotoi* blooms.

7 Conclusion

A species specific model for *Karenia mikimotoi* has been developped and inserted in a 3D model of primary production. Such refined ecosystem models focused on a species of interest are few and mainly focused on microalgae (eg. *Phaeocystis*, Lacroix *et al.*, 2007) or macroalgae (eg. *Ulva*, Ménesguen *et al.*, 2006) responsible for eutrophication disturbance.

The sensitivity of *Karenia mikimotoi* to agitation was taken into account through the shear rate (γ) in the mortality calculation as first suggested by Gentien (1998) and adapted by Loyer *et al.* (2001) in the 3D ecosystem model of the Bay of Biscay. In adding to the original processes described by Loyer *et al.* (2001), our model describes the detrimental effect of the production of exotoxins on the growth of co-occurring phytoplankton species (r_{all}).

This model reproduces blooms at the subsurface level and highlights the importance of the two major factors in *K. mikimotoi* dynamics : lower turbulence and stratification. The exceptional warm conditions in June 2003 produced a massive bloom. The results show that the model is very sensitive to its paramerization. Growth (through f_T) and mortality (through α) are strongly modulated by the water temperature. Sensitivity simulations highlight the key-role played by agitation for the spatial distribution of the bloom. Moreover, the *K. mikimotoi* biomass is doubled due to allelopathy exerted on competitors for resources. Although the spatial distribution of the computed *Karenia mikimotoi* shows a satisfactory accordance with Corystes data, the computed cell densities are lower. The simulated bloom does not exceed the hivernal nitrogen pool, whereas field population did. This may be due to swimming behaviour as has been investigated for *Karenia brevis* by (Liu *et al.*, 2002) in the Florida shelf region. Modelling dark-uptake of nitrogen (done by Yanagi *et al.*, 1995) or temporarily intracellular storage of nutrients may increase the biomass. However, this requires the use of quota model. In contrast to derived-Monod models, quota models consider that growth not only depends on the extracellular nutrient concentration, but also on the internal pool of nutrients (Ménesguen and Hoch, 1997; Flynn, 2003). The disadvantage being that quota models increase considerably the number of prognostic variables and consequently the computing time. Thus, in spite the limits of application of Monod models for the modelling of multi-nutrient interactions in phytoplankton (Droop, 1975; Flynn, 2003), it is these models that are still being coupled to circulation models. Thus, processes that would increase the *Karenia mikimotoi* biomass at the subsurface level can't actually be replicated with 3D refined ecosystem models as the computing time is still a strong constraint.

As well as the limitations in the models dynamics, it could be that interannual variability of fresh water intrusions from the Atlantic shelf could directly effect the bloom intensity (Kelly-Gerreyn *et al.*, 2005). This interesting hypothesis could be tested by further extending the model domain in addition to possesing increased knowledge of the location of over wintering populations.

Acknowledgements

This study was part of a project managed by Alain Lefevre (IFREMER/LER, Boulogne-sur-mer) and funded by IFREMER, the Région Nord-Pas de Calais and the national program 'PNEC-Chantier Manche orientale'. We thank Franck Dumas for the improvement of the circulation model MARS3D for this study. We are indebted also to Sophie Loyer for her advice concerning the *Karenia mikimotoi* submodel and her comments on the paper. The authors would like to thank Dr Matthew Frost from the Marine Environmental Change Network (MECN) to have communicated bottom and surface temperature at Station E1 for 2003. Hervé Roquet (METEO-FRANCE/CMS) facilitated the access to METEOSAT/AJONC products. The SeaWiFS images are available through a GMES service browser at : `http://www.ifremer.fr/cersat/facilities/browse/del/roses/browse.htm`. In addition we would like to thank Romain de Joux for his help in plotting the majority of the figures. L.Fernand and the Corsystes cruises were funded by UK Department DEFRA under project AE1225.

Appendix A - Processes linked to the plankton in the biogeochemical model.

The effect of the temperature f_T is an exponential function with a doubling of the effect for each 10 $^\circ$ C variation (Q_{10}=2): $f_T = exp^{a\ T}$, with T the water temperature.

Growth of the phytoplankton μ_i (d^{-1}), with i=Dia, Din, Nan : $\mu_i = \mu_i 0\ \ f_T\ \ f_{lim_i}$

The limiting effect f^i_{lim} is a Liebig low extended to the effect of light :

Dia : $f^i_{lim} = min(f^i_{lum}, f^i_N, f^i_{Si}, f^i_P)$ Din and Nan : $f^i_{lim} = min(f^i_{lum}, f^i_N, f^i_{Si}, f^i_P)$

The effet of light at the depth z, $f_{lum_i}(z)$, is approched by Steele (1962)'s formula :

$f^i_{lum}(z) = \frac{1}{\Delta z}\int_{z-\frac{1}{2}\Delta z}^{z+\frac{1}{2}\Delta z}\left(\frac{I_z/PAR}{I^i_{opt}}\right)\ exp^{\left(1-\frac{I_z/PAR}{I^i_{opt}}\right)}\ dz$, with I_{opt_i} the optimal irradiance of i.

From the sea surface irradiance I_0, the irradiance decreases exponentially : $I_z = I_0\ \ exp^{-k\ z}$

The extinction coefficient k is a combination of chlorophyll and SPM concentration (Gohin *et al.*, 2005) : $k = k_w + k_p\ \ Chl^{0.8} + k_{spm}\ \ SPM$

with k_w, k_p and k_{spm} are respectively the k of water, phytoplankton and mineral SPM.

The limiting effect exerted by each nutrient is described by a Michaelis-Menten relationship : for a nutrient n of concentration C_n : $f^i_n = \frac{C^i_n}{C_n + K^i_n}$; for nitrogen, it takes into account the both DIN forms : $f^i_N = f^i_{NO3} + f^i_{NH4} = \frac{NO_3}{NO_3 + K^i_{NO_3} + NH_4\ \frac{K^i_{NO_3}}{K^i_{NH_4}}} + \frac{NH_4}{NH^i_4 + K_{NH^i_4} + NO_3\ \frac{K^i_{NH_4}}{K^i_{NO_3}}}$

Death of the phytoplankton m_i (d^{-1}), with i=Dia, Din, Nan : $m_i = m0_i\ \ f_T$

Growth of the zooplankton μ_j (d^{-1}), with j=Mez, Miz :

For Mez, it is described by an Ivlev function :

$\mu_{Mez} = \mu 0_{Mez}\ \ f_T\ \ \left(1 - exp^{(-\gamma\ \ max(0, P^{Mez} - \delta))}\right)$

with $\mu 0_{Mez}$: the growth rate at 0 $^\circ$, δ : the escape threshold, P^{Mez} the available preys and γ : the slope of the Ivlev function.

For Miz it is described by a Michaelis-Menten function : $\mu_{Miz} = \mu 0_{Miz}\ \ f_T\ \ \frac{P^{Miz}}{P^{Miz} + k_{prey}}$

The available quantity of preys for each zooplankton class j is assessed with preferency factors :

$P_j = \sum p^i_j\ \ j$, with for Mez, i=Dia, Din, Miz and for Miz, i=Nano,Det

The assimilation rate of zooplankton is approached by : $\tau_j = 0.3\ \left(3 - 0.67\ \frac{P^j}{\mu 0_j\ \ f_T}\right)$.

Excretion of the zooplankton e_j (d^{-1}), with $j = \mathsf{Mez}, \mathsf{Miz}$: $e_j = e0_j\ \ f_T$

Death of the zooplankton m_j (d^{-1}), with $j = \mathsf{Mez}, \mathsf{Miz}$:

For Miz, it's only linked to the temperature : $m_{Miz} = m0_{Miz}\ \ f_T$

For Mez, it's also dependant of its biomass : $m_{Mez} = f_T\ \ max(m0_{Mez}, mb0_{Mez}\ \ \mathsf{Mez})$

Appendix B - Processes linked to the suspended feeders, detrital matters and sinking processes in the biogeochemical model.

Uptake of phytoplankton and detritus by suspension feeders u_{Bent} $(\mu mol\ N\ l^{-1}\ d^{-1})$:

It is dependant of a seasonal filtration intensity $(fsin(t))$ and of the prey availability (P_{Bent}) :

$u^q_{Bent}(t) = fil_{max}\ \ fsin(t)\ \ f_P\ \ P^q_{Bent}$, with $q = (Phy, Det)$.

$P^{Phy}_{Bent} = \sum i$, with i=Dia, Din, Nan and $P^{Det}_{Bent} = min(\mathsf{Ndet}, \mathsf{Pdet}\ \ r^{Det}_{N:P})$.

With t the julian day : $fsin(t) = \big(1 + sin\ (\frac{2\ \pi}{365}\ \ (t - 125))\big)/2$

Preys escape to the grazing pressure following a Michaelis-Menten function : $f_P = \frac{P_{Bent}}{P_{Bent}+K_{Bent}}$

Mortality m_{Bent} **and excretion** e_{Bent} **of suspension feeders** (d^{-1}) :

The mortality is dependant of the benthos biomass : $m^{Bent} = f_T\ \ max(m0_{Bent}, mb0_{Bent}\ \ \mathsf{Bent})$

The dissolved excretion kinetics is only moduled by temperature : $e_{Bent} = f_T\ \ e0_{Bent}$

The **sedimentation velocity of diatoms** w^{Dia} $(m\ d^{-1})$ depends of the nutrient limitation f_{Nlim} : $w^{Dia} = w^{Dia}_{min}\ \ {f_{Nlim}}^{0.2} + w^{Dia}_{max}\ \ \big(1 - {f_{Nlim}}^{0.2}\big)$, with $f_{Nlim} = min(f_N, f_P, f_{Si})$.

Sedimentation velocity of detrital matters w^{Det} $(m\ d^{-1})$:

$w^{Det} = w^{Det}_{Zoo}\ \ \left(\frac{1}{r+1}\right) + w^{Det}_{Phy}\ \ \left(1 - \frac{1}{r+1}\right)$, with $r = Q_{phyto}/Q_{Zoo}$

$Q_{phyto} = \sum_{i=1}^{4} m_i\ \ i$, with i=Dia, Din, Nan, Kar.

$Q_{Zoo} = \sum_{j=1}^{2}\big((1 - \tau_i)\ \ \mu_j + m_j\big)\ \ j$, with j=Mez, Miz.

w^{Det}_{Zoo} is a constant, but w^{Det}_{Phyto} is driven by the Stockes law (Yamamoto, 1983) :

$w^{Det}_{Phyto} = \frac{1}{18}\ \ g\ \ r_{Det}\ \ \frac{\rho_{Det}-\rho_w}{\nu\ \ \rho_w}$

with g the gravitational acceleration, ρ_{Det} the density of detrital particles of phytoplanktonic origin, r_{Det} the radius of these particles, ρ_w the water density and ν the molecular viscosity.

Adsorption and desorption of phosphate (d^{-1}) :

$k_{adsorp} = C_{adsorp}\ \ max(0\ ,\ C^{max}_{adsorp}\ \ \mathsf{SPM} - \mathsf{Pads})\quad k_{desorp} = C_{desorp}\ \ min(1\ ,\ \frac{\mathsf{Pads}}{C^{max}_{adsorp}\ \ \mathsf{SPM}})$

Remineralization of detrital matters in water and sediment (c: water w or sediment s) :

Remineralization of N and P in water : $minN_w = minN0_w\ \ f_T\qquad minP_w = minP0_w\ \ f_T$

Nitrification in water : $nit_w = nit0_w\ \ f_T$

In sediment, remineralization of nitrogen and phosphorus are drived by the oxic condition :

$minN_s = minN0_s\ \ f_T\ \ f^{min}_{\mathsf{O_2}}$, $minP_s = minP0_s\ \ f_T\ \ f^{min}_{\mathsf{O_2}}$, $nit_s = nit0_s\ \ f_T\ \ f^{nit}_{\mathsf{O_2}}$

with $f^{min}_{\mathsf{O_2}} = \mathsf{O_2}/(\mathsf{O_2} + K^{min}_{\mathsf{O_2}})$ and $f^{nit}_{\mathsf{O_2}} = \mathsf{O_2}/(\mathsf{O_2} + K^{nit}_{\mathsf{O_2}})$

Dissolution of biogenic silicon : $disSi_c = disSi0_c\ \ f_T$

References

Aksnes D., Ulvestad K., Balino B., Berntsen J., Egge J., Svendsen E., 1995. Ecological modelling in coastal waters : towards predictive physical-chemical-biological simulation models. Ophelia, 41: 5–36.

Allen J. I., Blackford J., Holt J., Proctor R., Ashworth M., Siddorn J., 2001. A highly spatially resolved ecosystem model for the North West European Continental Shelf. Sarsia, 86: 423–440.

Andersen V., Nival P., 1989. Modelling of phytoplankton population dynamics in an enclosed water column. J. Mar. Biol. Assoc. UK, 69: 625–646.

Anderson D., 1997. Turning back the harmful red tide. Nature, 388: 513–514.

Anderson T., Williams P., 1998. Modelling the seasonal cycle of dissolved organic carbon at station E1 in the English Channel. Est. Coast. Shelf Sci., 46: 93–109.

Arhonditsis George B., Brett Michael T., 2004. Evaluation of the current state of mechanistic aquatic biogeochemical modeling. Mar. Ecol. Prog. Ser., 271: 13–26.

Arzul G., Erard-Le Denn E., Videau C., Jégou A. M., Gentien P., 1993. Diatom growth repressing factors during an offshore bloom of *Gyrodinium* cf. *aureolum*, vol. 283, pp. 365–367.

Arzul G., Erard-Le Denn E., Belin C., Nézan E., 1995. Ichtyotoxic events associated with *Gymonodinium* cf. *nagasakiense* on the Atlantic coast of France. Harmful Algal News, 2–3: 8–9.

Azam F., Fenchel T., Field J., Gray J., Meyer-Reil L., Thingstad F., 1983. The ecological role of water-column microbes in the sea. Mar. Ecol. Prog. Ser., 10: 257–263.

Baretta J., Ebenhöh W., Ruardij P., 1995. The European Regional Seas Ecosystem Model, a complex marine ecosystem model. Neth. J. Sea Res., 33: 233–246.

Baretta-Becker J., Riemann B., Baretta J., Koch-Ramsmussen E., 1994. Testing the microbial loop concept by comparing mesocosm data with results from a dynamical simulation model. Mar. Ecol. Prog. Ser., 106: 187–198.

Baretta-Bekker J. G., Baretta J. W., Hansen A. S., Riemann B., 1998. An improved model of carbon and nutrient dynamics in the microbial food web in marine enclosures. Aquatic Microbial Ecology, 14: 91–108.

Birrien J.-L., Wafar M. V., Le Corre P., Riso R., 1991. Nutrients and primary production in a shallow stratified ecosystem in the Iroise Sea. J. Plank. Res., 13 (4): 1251–1265.

Bjoernsen P. K., Nielsen T. G., 1991. Decimeter scale heterogeneity in the plankton during a pycnocline bloom of *Gyrodinium aureolum*. Mar. Ecol. Prog. Ser., 73: 262–267.

Blasco D., Berard-Therriault L., Levasseur M., Vrieling E., 1996. Temporal and spatial distribution of the ichthyotoxic dinoflagellate *Gyrodinium aureolum* Hulburt in the St Lawrence, Canada. Journal of Plankton Research, 18 (10): 1917–1930.

Brisson A., Le Borgne P., Marsouin A., Moreau T., 1994. Surface irradiance calculated from Meteosat sensor during SOFIA-ASTEX. Int. J. Remote Sens., 15: 197–204.

Brisson A., Le Borgne P., Marsouin A., 1996. Operational surface solar irradiance using Meteosat data : Routine calibration and validation results. In : 1996 Meteorological satellite data users' conference EUMETSAT, pp. 229–238. 16-20 September 1996, Wien, Austria.

Brylinski J.-M., Lagadeuc Y., Gentilhomme V., Dupont J.-P., Lafite R., Dupeuble P.-A., Huault M.-F., Auger Y., Puskaric E., Wartel M., Cabioch L., 1991. Le "Fleuve côtier" : un phénomène hydrologique important en Manche orientale. Exemple du Pas-de-Calais. In : Chamley H., (Ed.), Actes du Colloque International sur l'Environnement des mers épicontinentales. Oceanologica Acta, vol. sp. (11): 197–203.

Chrétiennot-Dinet M.-J., 1998. Global increase of algal blooms, toxic events, casual species introductions and biodiversity. Oceanis, 24 (4): 223–238.

Cugier P., Le Hir P., 2000. Modélisation 3D des matières en suspension en baie de Seine orientale (Manche, France). C.R. Acad. Sci. Paris, Sciences de la Terre et des Planètes, 331: 287–294.

Cugier P., Billen G., Guillaud J. F., Garnier J., Ménesguen A., 2005a. Modelling the eutrophication of the Seine Bight (France) under historical, present and future riverine nutrient loading. Journal of Hydrology, 304: 381–396.

Cugier P., Ménesguen A., Guillaud J.-F., 2005b. Three dimensional (3D) ecological modelling of the Bay of Seine (English Channel, France). J. Sea Res., 54: 104–124.

Daugbjerg N., Hansen G., Larsen J., Moestrup O., 2000. Phylogeny of some of the major genera of dinoflagellates based on ultrastructure and partial LSU rDNA sequence data, including the erection of three new genera of unarmoured dinoflagellates. Phycologia, 39 (4): 302–317.

Dixon G. K., Holligan P. M., 1989. Studies on the growth and nitrogen assimilation of the bloom dinoflagellate *Gyrodinium aureolum* Hulburt. Journal of Plankton Research, 11 (1): 105–118.

Droop M., 1975. The nutrient status of algal cells in batch culture. Journal of Marine Biological Association U.K., 55: 541–555.

Ebenhöh W., Baretta-Bekker J., Baretta J., 1997. The primary production module in the marine ecosystem model ERSEM II, with emphasis on the light forcing. J. Sea Res., 38: 173–193.

Erard-Le Denn E., Belin C., Billard C., 2001. Various cases of ichtyotoxic blooms in France. In : Arzul G., (Ed.), Aquaculture environement and marine phytoplankton. 21-23 May 1992, Brest (France).

Fistarol G. O., Legrand C., Rengefors K., Granéli E., 2004. Temporary cysts formation in phytoplankton : a response to allelopathic competitors ? Environmental Microbiology, 6 (8): 791–798.

Flynn K. J., 2003. Modelling multi-nutrient interactions in phytoplankton; balancing simplicity and realism. Progress in Oceanography, 56: 249–279.

Garcia V. M., Purdie D. A., 1992. The influence of irradiance on growth, photosynthesis and respiration of *Gyrodinium* cf. *aureolum*. J. Plank. Res., 14 (9): 1251–1265.

Garcia V. M., Purdie D. A., 1994. Primary production studies during a *Gyrodinium* cf. *aureolum* (Dinophyceae) bloom in the western English Channel. Marine Biology, 119 (2): 297–305.

Gentien P., 1998. Bloom dynamics and ecophysiology of the *Gymnodinium mikimotoi* species complex. In : Anderson D. M., Cembella A. D., Hallegraef G. M., (Ed.), Physiological Ecology of Harmful Algal Blooms, vol. G 41, pp. 155–173. NATO ASI Series. Springer-Verlag.

Gohin F., Druon J.-N., Lampert L., 2002. A five channel chlorophyll concentration algorithm applied to SeaWiFS data processed by Sea DAS in coastal waters. Int. J. Remote Sensing, 23 (8): 1639–1661.

Gohin F., Loyer S., Lunven M., Labry C., Froidefond J.-M., Delmas D., Huret M., Herbland A., 2005. Satellite-derived parameters for biological modelling in coastal waters : illustration over the eastern continental shelf of the Bay of Biscay. Remote Sens. Environ., 95 (1): 29–46.

Granéli E., 2004. Eutrophication and Harmful Algal Blooms. In : Wassman P., Olli K., (Ed.), Drainage basin nutrient inputs and eutrophication : an integrated approach, incollection 7, pp. 99–112.

Guillaud J.-F., Andrieux F., Ménesguen A., 2000. Biochemical modelling in the Bay of Seine (France): an improvement by the introducing phosphorus in nutrient cycles. J. Mar. Sys., 25: 369–386.

Hansen P. J., Granéli E., Legrand C., Salomon G., Skovgaard A., 2003. Allelopathy and mixotro-

phy among bloom forming algae : Kill or eat your competitor. In : Hallegraeff G., Blackburn S. I., Bolch C., Lewis R., (Ed.), EUROHAB workshop 2003, pp. 40–42. 17-18 March 2003, Amsterdam.

Hashioka Y., Yamanaka Y., 2007. Seasonal and regional variations of phytoplankton groups by top-down and bottom-up controls obtained by a 3D ecosystem model. Ecological Modelling, 202: 68–80.

Hoch T., 1998. Modélisation du réseau trophique pélagique et de la production primaire en Manche. Oceanol. Acta, 21 (6): 871–885.

Hoch T., Garreau P., 1998. Phytoplankton dynamics in the English Channel: a simplified three-dimensional approach. J. Mar. Syst., 16: 133–150.

Hoch T., Ménesguen A., 1997. Modelling the biogeochemical cycles of elements limiting the primary production in the Channel. II. Sensivity analysis. Mar. Ecol. Prog. Ser., 146: 189–205.

Hodgkiss I., Yang Z., 2001. New and dominant species from Sam Xing Wan, Sai Kung during the 1998 massive killing red tide in Hong Kong. In : Hallegraeff G. M., Blackburn S. I., Bolch C. J., Lewis R. J., (Ed.), Harmful Algal Blooms 2000, pp. 62–65.

Holligan P. M., 1979. Dinoflagellate blooms associated with tidal fronts around the Brittish Iles. In : Taylor D. L., Seliger Howard H., (Ed.), International conference on Toxic Dinoflagellate blooms, 31 Oct. - 5 Nov. 1978, Key Biscayne (Florida), pp. 249–256. Elsevier, New York.

Holligan P. M., Harris R. P., Newell R. C., Harbour D. S., Head R. N., Linley E. A., Lucas M. I., Tranter P. R., Weekley C. M., 1984. The vertical distribution and partitioning of organic carbon in mixed, frontal and stratified waters of the English Channel. Mar. Ecol. Prog. Ser., 14: 111–127.

Holt J., James I., 2001. An *s* coordinate density evolving model of the northwest European continental shelf. 1. Model description and density structure. J. Geophys. Res., 106 (C7): 14,015–14,034.

Huret M., 2005. Apports des données "couleur de l'eau" à la modélisation couplée physique-biogéochimie en milieu dynamique côtier. Ph.D. thesis, Université de Toulouse III, p. 269.

Huret M., Gohin F., Delmas D., Lunven M., Garçon V., 2007. Use of the SeaWiFS data for improving the simulation of winter to spring phytoplankton production in the Bay of Biscay. J. Mar. Syst., 65 (1-4): 509–531.

Jenkinson I., Arzul G., 1998. Effect of the flagellates, *Gymnodinium mikimotoi*, *Heterosigma akashiwo* and *Pavlova lutheri*, on flow through fish gills. In : Reguera G., Blanco J., Fernandez M., Wyatt T., (Ed.), Harmful Microalgae, pp. 425–428.

Jenkinson I., Arzul G., 1999. Rôles de la rhéologie et des effets liés à l'activité cytolytique dans la dynamique et l'action toxique de *Gymnodinium mikimotoi* et d'autres algues nuisibles. Rapport final du PNEAT 1998-1999. Tech. report, ACRO-IFREMER.

Jenkinson I., Arzul G., 2001. Mitigation by cysteine compounds of rheotoxicity, ctytotoxycity and fish mortalities caused by the dinoflagellates, *Gymonidinium mikimotoi* and *G.* cf. *maguelonnense*. In : Hallegraeff G. M., Blackburn S. I., Bolch C. J., Lewis R. J., (Ed.), Harmful Algal Blooms 2000, pp. 461–464.

Jitts H. R., Morel A., Saijo Y., 1976. The relation of oceanic primary production to available photosynthetic irradiance. Austral. J. Mar. Fresh. Res., 27: 441–454.

Jones K. J., Ayres P., Bullock A. M., Roberts R. J., Tett P., 1982. A red tide of *Gyrodinium aureolum* in sea lochs of the Firth of Clyde and associated mortality of pond-reared salmon. J. Mar. Biol. Assoc. U.K., 62: 771–782.

Jordan M. B., Joint I., 1998. Seasonal variations in nitrate:phosphate ratios in the English

Channel 1923-1987. Estuarine, Coastal and Shelf Science, 46: 157–164.
Jørgensen S. E., 1999. State-of-the-art of ecological modelling with emphasis on development of structural dynamic models. Ecological Modelling, 120: 75–96.
Kelly-Gerreyn B. A., Qurban M. A., Hydes D. J., Miller P., Fernand L., 2004. Coupled "FerryBox" Ship of Opportunity and satellite data observations of plankton succession across the European shelf sea and Atlantic Ocean. In : Annual ICES Science Conference, 22-25 September 2004, Vigo, vol. CM 2004/P:28.
Kelly-Gerreyn B. A., Hydes D. J., Fernand L. J., Jégou A.-M., Lazure P., Puillat I., 2005. Low salinity intrusions in the western English Channel and possible consequences for biological production. Continental Shelf Research, in press.
Kholmeier C., Ebenhöh W., 2007. Modelling the ecosystem dynamics and nutrient cycling of the Spiekeroog back barrier system with a coupled EulerLagrange model on the base of ERSEM. Ecological Modelling, 202: 297–310.
Kubanek J., Hicks M. K., 2005. Does the red tide dinoflagellate *Karenia brevis* use allelopathy to outcompete other phytoplankton ? Limonol. Oceanogr., 50 (3): 883–895.
Lacroix G., Ruddick K., Ozer J., Lancelot C., 2004. Modelling the impact of the Scheldt and Rhine/Meuse plumes on the salinity distribution in Belgian waters (southern North Sea). J. Mar. Res., 52 (3): 149–153.
Lacroix G., Ruddick K., Gypens N., Spitz Y., Lancelot C., 2007. Validation of the 3D ecosystem model MIRO&CO with in situ measurements and MERIS-derived surface chlorophyll a images. 64 (1–4): 66–88.
Lancelot C., 1995. The mucilage phenomenon in the continental coastal waters in the North Sea. The Science of Total Environement, 165: 83–102.
Lancelot C., Spitz Y., Gypens N., Ruddick K., Becquevort S., Rousseau V., Lacroix G., Billen G., 2005. Modelling diatom-*Phaeocystis* blooms and nutrient cycles in the Southern Bight of the North Sea: the MIRO model. Mar. Ecol. Prog. Ser., 289: 63–78.
Lazure P., Dumas F., 2006. A 3D hydrodynamical model for applications at regional scale (MARS3D). Application to the Bay of Biscay. Advance in water ressources, submitted.
Lazure P., Jégou A.-M., 1998. 3D modelling of seasonal evolution of Loire and Gironde plumes on Biscay Bay continental shelf. Oceanologica Acta, 21: 165–177.
Le Corre P., L'Helguen S., Wafar M., 1993. Nitrogen source for uptake by *Gyrodinium* cf. *aureolum* in a tidal front. Limnol. Oceanogr., 38 (2): 446–451.
Le Fèvre-Lehoërff G., Erard-Le Denn E., Arzul G., 1993. Planktonic ecosystems in the Channel. Trophic relations. vol. 16, pp. 661–670.
Le Pape O., Ménesguen A., 1997. Hydrodynamic prevention of eutrophication in the Bay of Brest (France), a modelling approch. Journal of Marine Systems, 12: 171–186.
Le Pape O., Jean F., Ménesguen A., 1999. Pelagic and benthic trophic chain coupling in a semi-enclosed coastal system, the Bay of Brest (France) : a modelling approach. Marine Ecology Progress Series, 189: 135–147.
Lefebvre A., Libert A., 2003. Suivi régional des nutriments sur le littoral Nord / Pas de Calais / Picardie. Bilan de l'année 2003. techreport, IFREMER DEL/BL/TMR/02/05.
Liu G., Janowitz G., Kamykowski D., 2002. Influence of current shear on *Gymnodinium breve* (Dinophyceae) population dynamics: a numerical study. Marine Ecology Progress Series, 231: 47–66.
Lovejoy C., Bowman J., Hallegraeff G. M., 1998. Algicidal effects of a novel marine *Pseudoalteromonas* Isolate (Class *Proteobacteria*, Gamma Subdivision) on harmful algal bloom species of the genera *Chattonella*, *Gymnodinium*, and *Heterosigma*. Applied and Environmental Mi-

crobiology, Tome 13: 2806–2813.
Loyer S., 2001. Modélisation de la production phytoplanctonique dans la zone côtière atlantique enrichie par les apports fluviaux. Ph.D. thesis, Université de Paris VI, p. 256.
Loyer S., Lazure P., Gentien P., Ménesguen A., 2001. Modelling of *Gymnodinium mikimotoi* blooms along the French Atlantic coast : geographical and vertical distributions. Hydroécol. Appl., Tome 13 (volume 1): 57–76.
Ménesguen A., Hoch T., 1997. Modelling the biogeochemical cycles of elements limiting the primary production in the Channel. I. The role of thermohaline stratification. Mar. Ecol. Prog. Ser., 146: 173–188.
Ménesguen A., Guillaud J.-F., Hoch T., 1995. Modelling the eutrophication process in a river plume : the Seine case study (France). Ophelia, 42: 205–225.
Ménesguen A., Cugier P., Leblond I., 2006. A new numerical technique for tracking chemical species in a multi-source, coastal ecosystem, applied to nitrogen causing *Ulva* blooms in the Bay of Brest (France). Limnol. Oceanogr., 51 (1): 591–601.
Moll A., 1998. Regional distribution in the North Sea by a three-dimensional model. J. Mar. Sys., 16: 151–170.
Morin P., Birrien J.-L., Le Corre P., 1989. The frontal systems in the Iroise Sea : Development of *Gyrodinium aureolum* Hulburt on the inner front. Scient. Mar., 53 (02/03): 215–221.
Morquecho L., Lechuga-Devéze C. H., 2003. Dinoflagellate cysts in recent sediments from Bahía Concepción, Gulf of California. Botanica Marina, 46: 132–141.
Mortain-Bertand A., Descolas-Gros C., Jupin H., 1988. Growth, synthesis and carbon metabolism in the temperate marine diatom *Skeletonema costatum* adapted to low temperature and low photo-flux density. Marine Biology, 100: 135–141.
Moum J. N., Lueck R. G., 1985. Causes and implications of noise in oceanic dissipation measurements. Deep-Sea Res., 32: 379–392.
Mukhopadhyay B., Bhattacharyya R., 2006. Modelling phytoplankton allelopathy in a nutrient-plankton model with spatial heterogeneity. Ecological Modelling, 198: 163–173.
Ménesguen A., Aminot A., Belin C., Chapelle A., Guillaud J.-F., Joanny M., Lefebvre A., Merceron M., Piriou J.-Y., Souchu P., 2001. Tech. report. Rapport IFREMER DEL/EC/01.02 pour la Commission Européenne-DG.ENV.B1.
Onji M., Nakano S.-I., Suzuki S., 2003. Virus-like Particles Suppress Growth of the Red-Tide-Forming Marine Dinoflagellate *Gymnodinium mikimotoi*. Marine Biotechnology, 5 (5): 435–442.
Ottoway B., Parker M., D. M., Crowley M., 1979. Observations on a bloom of *Gyrodinium aureolum* Hulbert on the south coast of Ireland, summer 1976, associated with mortalities of littoral and sub-littoral organisms. Irish Fisheries Investigations, (18).
Paasche E., 1973. Silicon and the ecology of marine plankton diatoms. II Silicate-uptake kinetics in five diatom species. Mar. Biol., 19: 262–269.
Partensky F., Sournia A., 1986. Le dinoflagellé *Gyrodinium* cf. *aureolum* dans le plancton de l'Atlantique Nord : Identification, écologie, toxicité. Cryptogam. Algol., 7: 251–275.
Pastres R., Brigolin D., Petrizzo A., Zucchetta M., 2004. Testing the robustness of primary production models in shallow coastal areas : a case study. Ecological Modelling, 179: 221–233.
Persson A., 2000. Possible predation of cysts - a gap in the knowledge of dinoflagellate ecology. Journal of Plankton Research, 22 (4): 803–809.
Pingree R., 1975. The advance and retreat of the thermocline on the continental shelf. J. Mar. Biol. Ass. U.K., 55: 965–974.

Plus M., Deslous-Paoli J.-M., Auby I., Dagault F., 2003. Factors influencing primary production of seagrass beds (Zostera noltii hornem.) in the Thau lagoon (French Mediterranean coast). Journal of Experimental Marine Biology and Ecology, 259 (1): 63–84.

Plus M., La Jeunesse I., Bouraoui F., Zaldìvar J.-M., Chapelle A., Lazure P., 2006. Modelling water discharges and nitrogen inputs into a Mediterranean lagoon. Impact on the primary production. Ecological Modelling, 193: 69–89.

Prakash A., 1987. Coastal organic pollution as a contributing factor to red-tide development. techreport 187, Rapport et Procès-verbaux des Réunions, Conseil International pour l'Exploration de la Mer.

Prandle D., Loch S., Player R., 1993. Tidal flow through the Straits of Dover. J. of Physical Oceanography, 23 (1): 23–37.

Proctor R., James I. D., 1996. A fine-resolution 3D model of the southern North Sea. Journal of Marine Systems, 8: 285–295.

Purina I., Balode M., Béchemin C., Põder T., Verité C., Maestrini S., 2004. Influence of dissolved organic matter from terrestrial origin on the changes of dinoflagellates species composition in the Gulf of Riga, Baltic Sea. Hydrobiologia, 514: 127–137.

Quisthoudt C., 1987. Production primaire phytoplanctonique dans le détroit du Pas de Calais (France): variations spatiales et annuelles au large du Cap Gris-Nez. C. R. Acad. Sci., Paris, 304 (3): 245–250.

Raine R., O'Mahony J., McMahon T., Roden C., 1990. Hydrography and phytoplankton of waters off south-west Ireland. Estuarine, Coastal and Shelf Science, 30 (6): 579–592.

Raine R., Joyce B. R. J., Pazos Y., Moloney M., Jones K., Patching J., 1993. The development of a bloom of the dinoflagellate *Gyrodinium aureolum* (Hulbert) on the south-west Irish coast. ICES J. Mar. Sci., 50: 461–469.

Redfield A., Ketchum B., Ridchards F., 1963. The influence of organisms on the composition of sea water. In : Hill M. N., (Ed.), The Sea, vol. 2, pp. 26–77. Wiley Interscience, New-York.

Reynaud T., Legrand P., Mercier H., Barnier B., 1998. A new analysis of hydrographic data in the Atlantic and its application to an inverse modelling study. Int. WOCE Newsletter, 32: 29–31.

Riegman R., 1998. Species composition of harmful algal blooms in relation to macronutrient dynamics. In : Anderson D. M., Cembella A. D., Hallegraef G. M., (Ed.), Physiological Ecology of Harmful Algal Blooms, vol. G 41, pp. 475–488. NATO ASI Series Springer-Verlag.

Rodrìguez F., Fernàndez E., Head R., Harbour D., Bratak G., Heldal M., Harris R., 2000. Temporal variability of viruses, bacteria, phytoplankton and zooplankton in the western English Channel off Plymouth. J. Mar. Biol. Ass. U. K., 80: 575–586.

Salomon J.-C., Guegueniat P., Orbi A., Baron Y., 1988. A lagrangian model for long term tidally induced transport and mixing. Verification by artificial radionucleide concentrations, pp. 384–394. Elsevier Applied Science Publishers.

Savina M., 2004. Modélisation écologique des populations de palourdes roses (*Paphia rhomboïdes*) et d'amandes de mer (*Glycymeris glycymeris*) en Manche. Ph.D. thesis, Université d'Aix-Marseille II, p. 200.

Sharples J., Moore C., Rippeth T., Holligan P., Hydes D., Fisher N., Simpson J., 2001. Phytoplankton distribution and survival in the thermocline. Limnol. Oceanogr., 46 (3): 486–496.

Skogen M., Svendsen E., Berntsen J., Aksnes D., Ulvestad K., 1995. Modelling the primary production in the North Sea using a coupled 3 dimensional Physical Chemical Biological Ocean model. Est. Coast. Shelf Sci., 41: 545–565.

Smayda T. J., 2002. Turbulence, watermass stratification and harmful algal blooms : an alter-

native view and frontal zones as "pelagic seed banks". Harmful Algae, 1: 95–112.
Smith S. L., Yamanaka Y., 1996. Quantitative comparison of photoacclimation models for marine phytoplankton. Ecological Modelling, 201: 547–552.
Solé J., García-Ladona E., Ruardij P., Estrada M., 2005. Modelling allelopathy among marine algae. Ecological Modelling, 183: 373–384.
Sournia A., 1995. Red tide and toxic marine phytoplankton of the world's oceans : an inquiry into biodiversity. In : Lassus P., Arzul G., Erard E., Gentien P., Marcaillou C., (Ed.), Harmful Marine Algal Blooms, pp. 103–112. Lavoisier.
Steele J., 1962. Environmental control of photosynthesis in the sea. Limnol. Oceanogr., 7 (2): 137–150.
Tuchkovenko Y. S., Lonin S. A., 2003. Mathematical model of the oxygen regime of Cartagena Bay. Ecol. Model., 165: 91–106.
Yamaguchi M., 1994. Physiological ecology of the red tide flagellate *Gymnodinium nagasakiense* (Dinophyceae). Mechanism of the red tide occurrence and its prediction. Bulletin of the Nansei National Fisheries Research Institute, 27: 251–394.
Yamaguchi M., Honjo T., 1989. Effects of temperature, salinity and irradiance on the growth of the noxious red tide flagellate *Gymnodinium nagasakiense* (Dinophyceae). Nippon Suisan Gakkaishi, 55 (11): 2029–2036.
Yamaguchi M., Itakura S., 1999. Nutrition and growth kinetics in nitrogen- or phophorus-limited cultures of the noxious red tide dinoflagellate *Gymnodinium mikimotoi*. Fisheries Science, 65 (3): 367–373.
Yamamoto S., 1983. Settling velocity and accumulation of silt-sized quartz grain in the water column of the deep sea: a conceptual approach. Bull. Coll. Sci. Univ., 36: 117–128.
Yanagi T., Yamamoto T., Koizumi Y., Ikeda T., Kamizono M., Tamori H., Yamaguchi M., 1995. A numerical simulation of red tide formation. Bulletin of the Nansei National Fisheries Research Institute, 6 (3): 269–285.
Yang Z. B., Hodgkiss I. J., 2001. Early 1998 massive fish kills and associated phytoplankton in Port Shelter waters, Hong Kong. In : Hallegraeff G. M., Blackburn S. I., Bolch C. J., Lewis R. J., (Ed.), Harmful Algal Blooms 2000, pp. 70–73.
Yoshinaga I., Kawai T., Ishida Y., 1995. Lysis of *Gymnodinium nagasakiense* by marine bacteria. In : Lassus P., Arzul G., Erard E., Gentien P., Marcaillou C., (Ed.), Harmful Marine Algal Blooms, pp. 687–692. Lavoisier.
Zharova N., Sfriso A., Voinov A., Pavoni B., 2001. A simulation model for the annual Âuctuation of Zostera marina in the Venice lagoon. Aquat. Bot., 70: 135–150.

List of Tables

List of Figures

$$\frac{d\mathsf{NH_4}}{dt} = minN_w \ \mathsf{Ndet} - nit \ \mathsf{NH_4} - r^{\mathsf{Kar}}_{NH4} \ \mu_{Kar} \ \mathsf{Kar} \ r^{Kar}_{N:cell} + r^{Zoo}_{N:dw} \sum_{j=\mathsf{Mez,\ Miz}} \left[e_j \ j\right]$$
$$- \sum_{i=\mathsf{Dia,\ Din,\ Nan}} \left[r^i_{NH4} \ \mu_i \ i\right] + \left[e_{Bent} \ \mathsf{Bent} \ M_C \ 10^{-3} \ / \left(r^{Bent}_{C:N} \ z_{(l)}\right)\right]^{l=1}$$
$$\frac{d\mathsf{NO_3}}{dt} = nit_N \ \mathsf{NH_4} - \sum_{i=\mathsf{Dia,\ Din,\ Nan}} \left[r^i_{NO3} \ \mu_i \ i\right] - r^{\mathsf{Kar}}_{NO3} \ \mu_{Kar} \ \mathsf{Kar} \ r^{Kar}_{N:cell}$$
$$\frac{d\mathsf{SiOH}}{dt} = disSi_w \ \mathsf{Sidet} - r^{Phy}_{Si:N} \ \mu_{Dia} \ \mathsf{Dia}$$
$$\frac{d\mathsf{PO_4}}{dt} = minP_w \ \mathsf{Pdet} + r_{P:N} \left[r^{Zoo}_{N:dw} \sum_{j=\mathsf{Mez,\ Miz}} \left[e_j \ j\right] - \sum_{i=\mathsf{Dia,\ Din,\ Nan}} \left[\mu_i \ i\right] + \mu_{Kar} \ \mathsf{Kar} \ r^{Kar}_{N:cell}\right.$$
$$\left. + \left[e_{Bent} \ \mathsf{Bent} \ M_C \ 10^{-3} \ / \left(r^{Bent}_{C:N} \ z_{(l)}\right)\right]^{l=1}\right] - k_{adsorp} \ \mathsf{PO_4} + k_{desorp} \ \mathsf{Pads}$$
$$\frac{d\mathsf{Pads}}{dt} = k_{adsorp} \ \mathsf{PO_4} - k_{desorp} \ \mathsf{Pads}$$
$$\frac{d\mathsf{Dia}}{dt} = (\mu_{Dia} - m_{Dia}) \ \mathsf{Dia} - \mu_{Mez} \ (p^{Dia}_{Mez} \ \mathsf{Dia}/P^{Mez}) \ \mathsf{Mez} \ r^{Zoo}_{N:dw} - u^{Phy}_{Bent} \ \left(\mathsf{Dia} \ / \ P^{Phy}_{Bent}\right)$$
$$\frac{d\mathsf{Din}}{dt} = (\mu_{Din} - m_{Din}) \ \mathsf{Din} - \mu_{Mez} \ (p^{Din}_{Mez} \ \mathsf{Din}/P^{Mez}) \ \mathsf{Mez} \ r^{Zoo}_{N:dw} - u^{Phy}_{Bent} \ \left(\mathsf{Din} \ / \ P^{Phy}_{Bent}\right)$$
$$\frac{d\mathsf{Nan}}{dt} = (\mu_{Nan} - m_{Nan}) \ \mathsf{Nan} - \mu_{Miz} \ (p^{Nan}_{Miz} \ \mathsf{Nan}/P^{Miz}) \ \mathsf{Miz} \ r^{Zoo}_{N:dw} - u^{Phy}_{Bent} \ \left(\mathsf{Nan} \ / \ P^{Phy}_{Bent}\right)$$
$$\frac{d\mathsf{Kar}}{dt} = \mu_{Kar} \ \mathsf{Kar} - m_{Kar} \ \mathsf{Kar}^2$$
$$\frac{d\mathsf{Ndet}}{dt} = \sum_{i=\mathsf{Dia,\ Din,\ Nan}} \left[m_i \ i\right] + m_{Kar} \ \mathsf{Kar} \ r^{Kar}_{N:cell} + \sum_{j=\mathsf{Mez,\ Miz}} \left[m_j + (1-\tau_j) \ \mu_j \ j\right] \ r^{Zoo}_{N:dw}$$
$$-minN_w \ \mathsf{Ndet} - \mu_{Miz} \ (p^{Det}_{Miz} \ \mathsf{Det}/P^{Miz}) \ \mathsf{Miz} \ r^{Zoo}_{N:dw}$$
$$-u^{Det}_{Bent} \ \tau_{Det} + u^{Phy}_{Bent} \ (1-\tau_{Phy}) + \left[m_{Bent} \ \mathsf{Bent} \ M_C \ 10^{-3} \ / \ (r^{Bent}_{C:N} \ z_{(l)})\right]^{l=1}$$
$$\frac{d\mathsf{Sidet}}{dt} = -disSi_w \ \mathsf{Sidet} + r_{Si:N} \left[(m_{Dia} \ \mathsf{Dia} + \mu^{Dia}_{Mez} \ (1-\tau_{Mez}) \ \mathsf{Mez} \ r^{Zoo}_{N:dw})\right.$$
$$\left. + \left[u^{Phy}_{Bent} \ \left(\mathsf{Dia} \ / \ P^{Bent}_{Phy}\right) \ (1-\tau_{Phy})\right]^{l=1}\right]$$
$$\frac{d\mathsf{Pdet}}{dt} = -minP_w \ \mathsf{Pdet} + r_{P:N} \left[\sum_{i=\mathsf{Dia,\ Din,\ Nan}} \left[m_i \ i\right] + m_{Kar} \ \mathsf{Kar} \ r^{Kar}_{N:cell}\right.$$
$$+ \left(\sum_{j=\mathsf{Mez,\ Miz}} \left[(m_j + \mu_j \ (1-\tau_j)) \ j\right] - \mu_{Miz} \ (p^{Det}_{Miz} \ \mathsf{Det}/P^{Miz}) \ \mathsf{Miz}\right) r^{Zoo}_{N:dw}$$
$$\left. + \left[m_{Bent} \ \mathsf{Bent} \ M_C \ 10^{-3} \ / \ (r^{Bent}_{C:N} \ z_{(l)}) - u^{Det}_{Bent} \ \tau_{Det} + u^{Phy}_{Bent} \ (1-\tau_{Phy})\right]^{l=1}\right]$$
$$\frac{d\mathsf{Mez}}{dt} = (\mu_{Mez} \ \tau_{Mez}) - e_{Mez} - m_{Mez}) \ \mathsf{Mez}$$
$$\frac{d\mathsf{Miz}}{dt} = (\mu_{Miz} \ \tau_{Miz}) - e_{Miz} - m_{Miz}) \ \mathsf{Miz} - \mu_{Mez} \ (p^{Miz}_{Mez} \ \mathsf{Miz}/P^{Mez}) \ \mathsf{Mez}$$
$$\frac{d\mathsf{Bent}}{dt} = (u^{Phy}_{Bent} \ \tau_{Phy} + u^{Det}_{Bent} \ \tau_{Det}) \ 10^3 \ 1/M_C \ r^{Bent}_{C:N} \ z_{(l=1)} - (e_{Bent} + m_{Bent}) \ \mathsf{Bent}$$

Table 1
Differential equations for local sources and sinks of the non-conservative variables in water.

symbol	parameter	value	unit	source
General				
a	coefficient in thermal effect	0.07	$(^\circ\,\mathrm{C})^{-1}$	Baretta-Becker *et al.*, 1994
$r_{P:N}$	P:N ratio	0.0625	$mol\ mol^{-1}$	Redfield *et al.*, 1963
M_C	molar mass of carbon	12	$g\ mol^{-1}$	
Phytoplankton				
$r_{N:Chl}$	N:chl-a ratio	0.6285	$mol\ \mu g\ l^{-1}$	Huret *et al.*, 2007
$r_{C:N}^{Phy}$	C:N ratio (*K. mikimotoi* execpted)	6.625	$mol\ mol^{-1}$	Redfield *et al.*, 1963
Diatoms				
$\mu 0_{Dia}$	growth rate at $0\,^\circ$ C	0.7	d^{-1}	Paasche, 1973
$m0_{Dia}$	mortality rate at $0\,^\circ$ C	0.03	d^{-1}	Cugier *et al.*, 2005b
K_{NO3}^{Dia}	half-saturation constant for NO_3	2	$\mu mol\ l^{-1}$	Andersen and Nival, 1989
K_{NH4}^{Dia}	half-saturation constant for NH_4	1.5	$\mu mol\ l^{-1}$	Loyer, 2001
K_P^{Dia}	half-saturation constant for P	0.15	$\mu mol\ l^{-1}$	Aksnes *et al.*, 1995
K_{Si}^{Dia}	half-saturation constant for Si	1	$\mu mol\ l^{-1}$	Paasche, 1973
I_{opt}^{Dia}	optimal irradiance	70	$W\ m^{-2}$	Mortain-Bertand *et al.*, 1988
$r_{Si:N}^{Dia}$	Si:N ratio	0.65	$mol\ mol^{-1}$	adjusted
Dinoflagellates				
$\mu 0_{Din}$	growth rate at $0\,^\circ$ C	0.35	d^{-1}	Cugier *et al.*, 2005b
$m0_{Din}$	mortality rate at $0\,^\circ$ C	0.02	d^{-1}	Cugier *et al.*, 2005b
K_{NO3}^{Din}	half-saturation constant for NO_3	4	$\mu mol\ l^{-1}$	Loyer, 2001
K_{NH4}^{Din}	half-saturation constant for NH_4	0.9	$\mu mol\ l^{-1}$	Loyer, 2001
K_P^{Din}	half-saturation constant for P	0.1	$\mu mol\ l^{-1}$	Aksnes *et al.*, 1995
I_{opt}^{Din}	optimal irradiance	170	$W\ m^{-2}$	Cugier *et al.*, 2005b
Nanophytoplankton				
$\mu 0_{Nan}$	growth rate at $0\,^\circ$ C	1	d^{-1}	Hoch, 1998
m_{Nan}	mortality rate	0.115	d^{-1}	adjusted
K_{N03}^{Nan}	half-saturation constant for NO_3	0.1	$\mu mol\ l^{-1}$	adjusted
K_{NH4}^{Nan}	half-saturation constant for NH_4	0.05	$\mu mol\ l^{-1}$	Loyer, 2001
K_P^{Nan}	half-saturation constant for P	0.1	$\mu mol\ l^{-1}$	Hoch, 1998
I_{opt}^{Nan}	half-sat. constant for irradiance	20	$W\ m^{-2}$	Loyer, 2001

Table 2
Parameters used for the general planktonic system (1/2).

symbol	parameter	value	unit	source
Coefficients for ligth attenuation				
PAR	photosynthetic active radiation coeff.	42.5	%	Jitts *et al.*, 1976
k_w	attenuation coefficient due to water	0.1	m^{-1}	Gohin *et al.*, 2005
k_p	attenuation coefficient due to chl-a	0.05	$m^{-1}(mg\ m^{-3})^{-1}$	Gohin *et al.*, 2005
k_{spm}	attenuation coefficient due to SPM	0.0625	$m^{-1}(mg\ l^{-1})^{-1}$	Gohin *et al.*, 2005
Karenia mikimotoi				
mc_{Kar}	mortality rate	$3.2\ 10^{-9}$	$cell\ l^{-1}$	Loyer, 2001
K_{N03}^{Kar}	half-saturation constant for NO_3	5	$\mu mol\ N\ l^{-1}$	Loyer *et al.*, 2001
K_{NH4}^{Kar}	half-saturation constant for NH_4	0.01	$\mu mol\ P\ l^{-1}$	Loyer *et al.*, 2001
K_P^{Kar}	half-saturation constant for P	0.05	$\mu mol\ Si\ l^{-1}$	Loyer *et al.*, 2001
I_{opt}^{Kar}	half-saturation constant for irradiance	1.15	$W\ m^{-2}$	Loyer, 2001
$r_{cell:chl}^{Kar}$	number of cells per unit of chl-a biomass	53,000	$cells\ \mu g^{-1}$	Corystes 8/03
$r_{N:cell}^{Kar}$	internal quota in N	$4\ 10^{-6}$	$pmol\ cell^{-1}$	adjusted
Common parameters of the Zooplankton				
$r_{C:dw}^{Zoo}$	C:dry weight ratio	0.25	$g\ g^{-1}$	LL93
$r_{C:N}^{Zoo}$	C:N ratio	5	$mol\ mol^{-1}$	LL93
Mesozooplankton				
$\mu 0_{Mez}$	growth rate at 0 ° C	0.3	d^{-1}	Hoch, 1998
$m0_{Mez}$	mortality rate at 0 ° C	0.06	d^{-1}	Cugier *et al.*, 2005b
$mb0_{Mez}$	biomass-dependant mortality rate at 0 ° C	0.0006	$d^{-1}\ (\mu g^{-1}\ l)$	Cugier *et al.*, 2005b
δ	predation escape threshold	0.75	$\mu mol\ N\ l^{-1}$	adjusted
τ_{Miz}	assimilation rate	0.6	$adim.$	Azam *et al.*, 1983
$e0_{Mez}$	excretion rate at 0 ° C	0.03	d^{-1}	Hoch, 1998
γ	slope of the Ivlev function	0.15	$l\ (\mu mol\ N)^{-1}$	adjusted
p_{Dia}	preferency coeficient for Dia	1.0	dimens. less	Loyer, 2001
p_{Din}	preferency coeficient for Din	0.1	dimens. less	Loyer, 2001
p_{Miz}	preferency coeficient for Miz	0.7	dimens. less	Loyer, 2001
Microzooplankton				
$\mu 0_{Miz}$	growth rate at 0 ° C	0.3	d^{-1}	Hoch, 1998
$m0_{Miz}$	mortality rate at 0 ° C	0.1	d^{-1}	Hoch, 1998
k_{prey}	half-saturation coefficient of preys	0.5	$\mu mol\ N\ l^{-1}$	adjusted
p_{Det}	preferency coeficient for detrital matters	0.8	dimens. less	adjusted
$e0_{Miz}$	excretion rate at 0 ° C	0.1	d^{-1}	Hoch, 1998

Table 3
Parameters used for the general planktonic system (2/2). LL93 : Le Fèvre-Lehoërff *et al.*, 1993

symbol	parameter	value	unit	source
fil_{max}	maximum filtration rate	15	$dm^3\ j^{-1}\ m^{-2}$	calibrated
$m0_{Bent}$	mortality rate at 0 ° C	0.001	d^{-1}	Le Pape *et al.*, 1999
$mb0_{Bent}$	biomass-dependant mortality at 0 ° C	0.0002	$d^{-1}\ (g\ m^{-2}C)^{-1}$	calibrated
$e0_{Bent}$	excretion rate at 0 ° C	0.0025	d^{-1}	calibrated
K_{Bent}	half-saturation constant for preys	0.5	$\mu mol\ l^{-1}\ N$	calibrated
τ_{Phy}	assimilation rate of phytoplankton	0.6	*adim.*	Le Pape *et al.*, 1999
τ_{Det}	assimilation rate of detrital matters	0.2	*adim.*	Le Pape *et al.*, 1999
$r^{Bent}_{C:N}$	C:N ratio of benthos	5	$mol\ mol^{-1}$	Le Pape *et al.*, 1999

Table 4
Parameters in relation to the benthic suspension feeders.

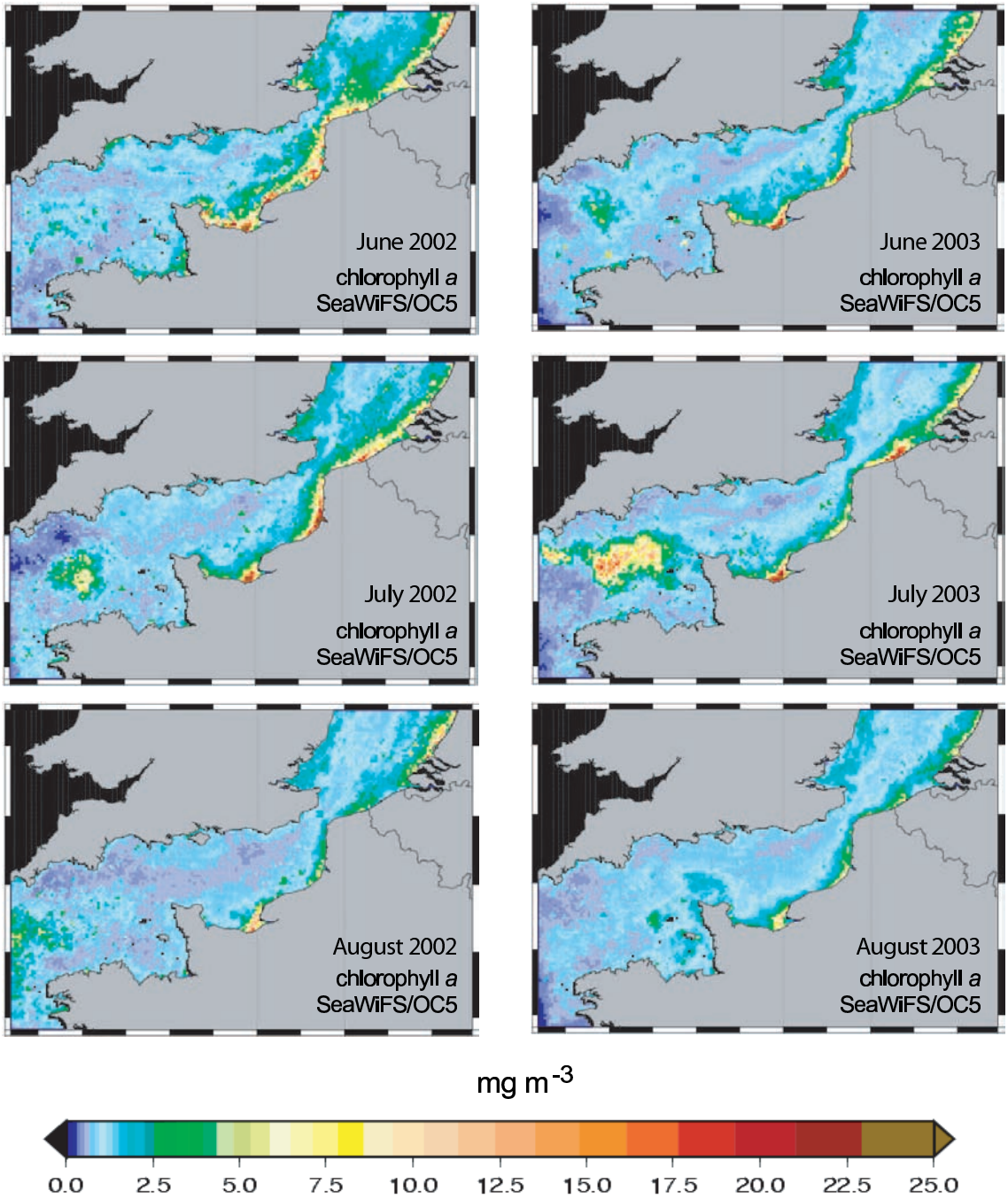

Fig. 1. Monthly composites of the sea surface chlorophyll *a* concentration derived from SeaWiFS/OC5.

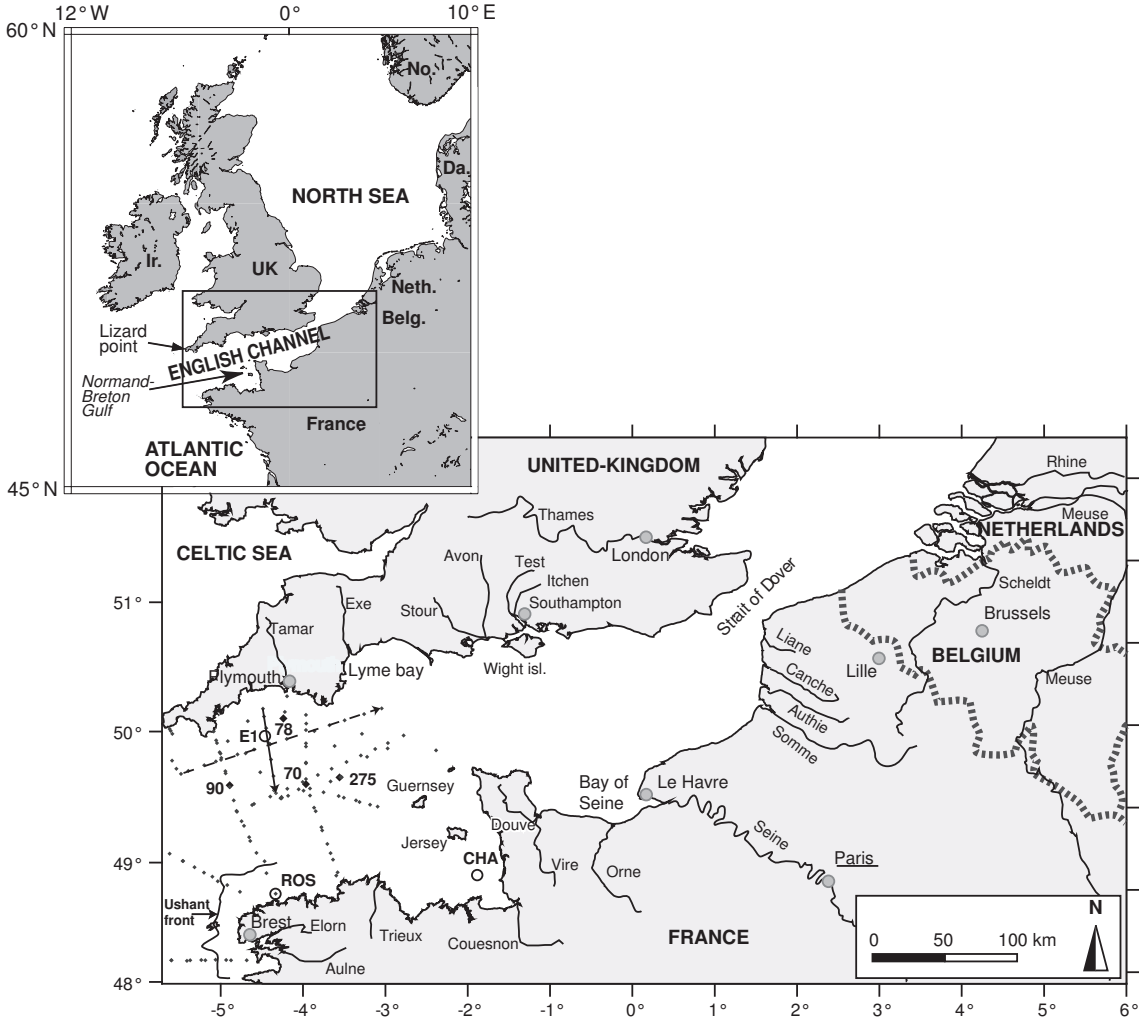

Fig. 2. Catchment of the model and rivers taken into account. Validation data used : • Cruise 08/03 (bigger and numbered particularly when used in the present paper), → : Scanfish leg 120 (same cruise), --→ : Scanfish leg 240 (same cruise), ∘ : additional stations from survey networks. The position of the Ushant Front is drawn after Pingree (1975).

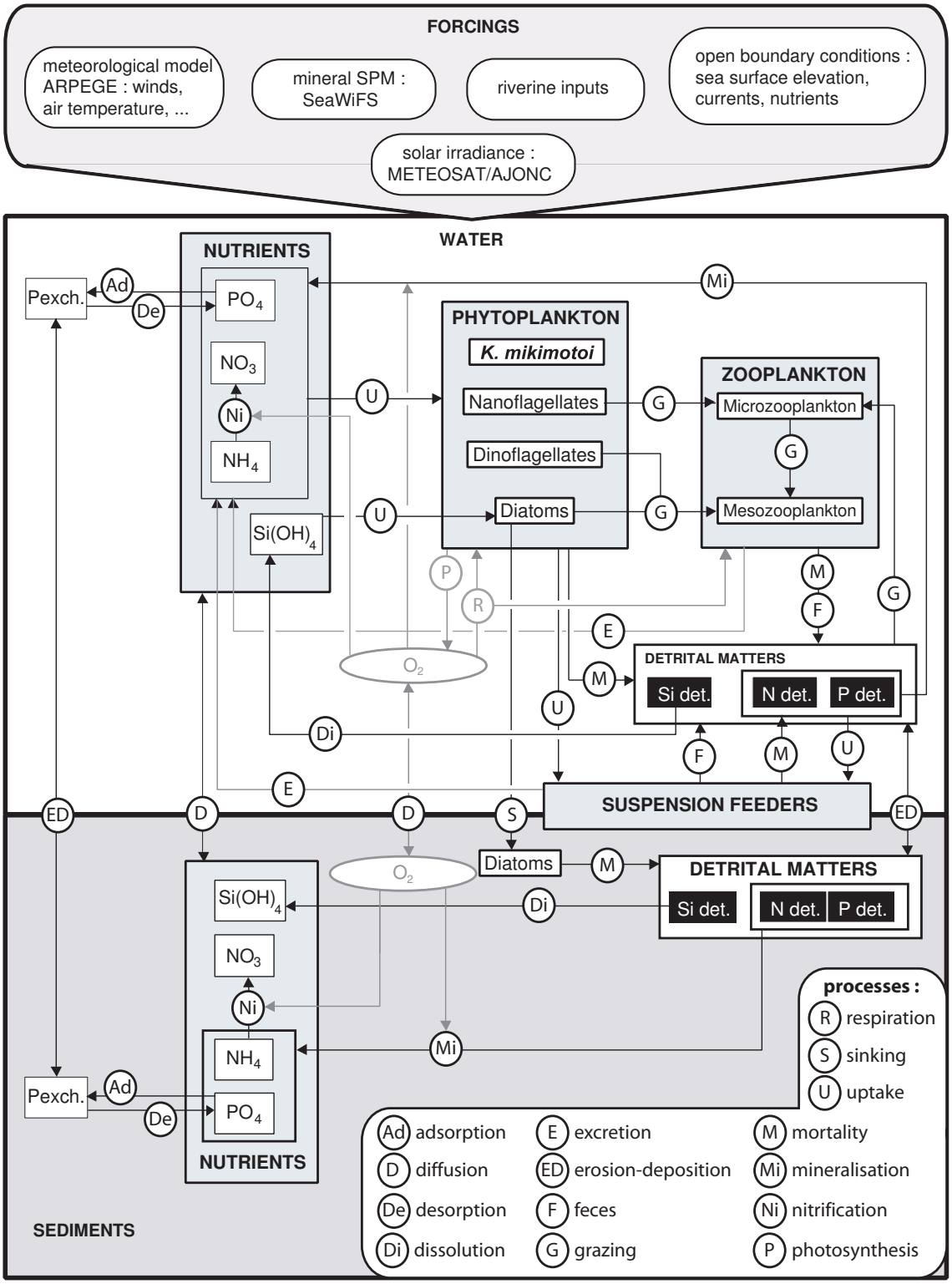

Fig. 3. Conceptual scheme of the ecological model and forcings.

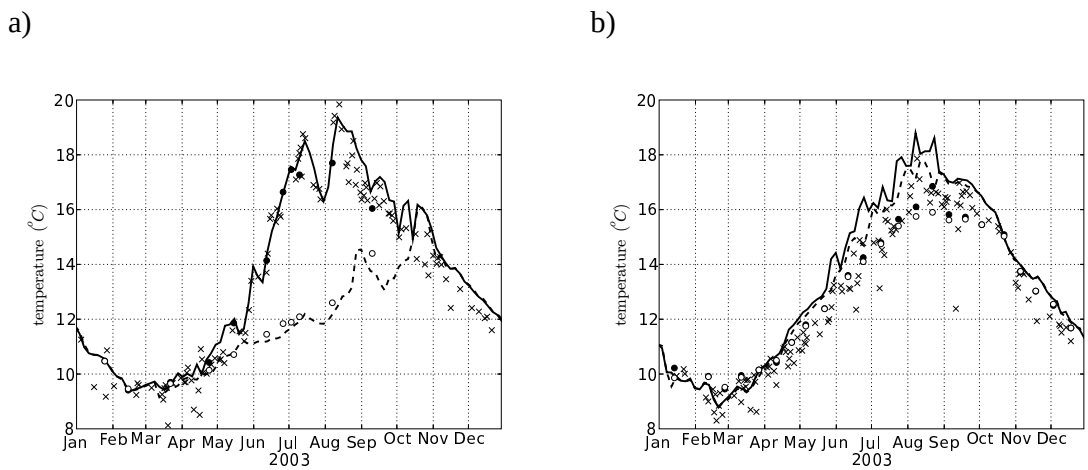

Fig. 4. Surface and bottom water temperature at Station E1 (a) and Station ROS (b) computed by the model (continuous and dashed lines respectively), from field data (surface : •, bottom : ○) and from AVHRR captor (×). E1 field data supplied by Marine Environmental Change Network and Marine Biological Association of the UK.

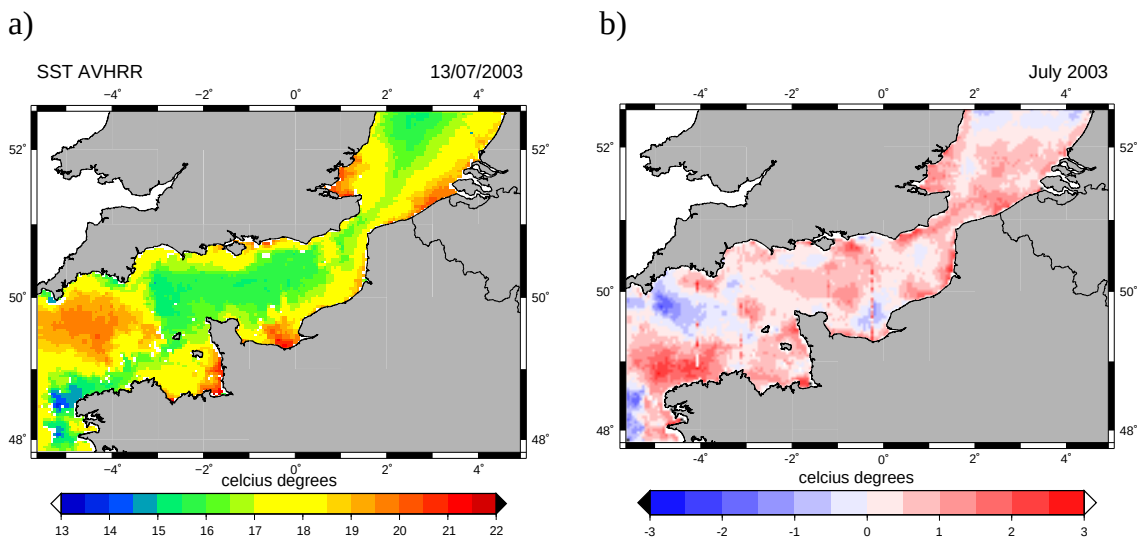

Fig. 5. SST from AVHRR captor on the 13 th of July 2003 (a) and difference between the model and the AVHRR captor in the assessment of the mean SST of July 2003 (b), red colorscale indicates areas of overestimation by the model, blue colorscale indicates areas of underestimation by the model.

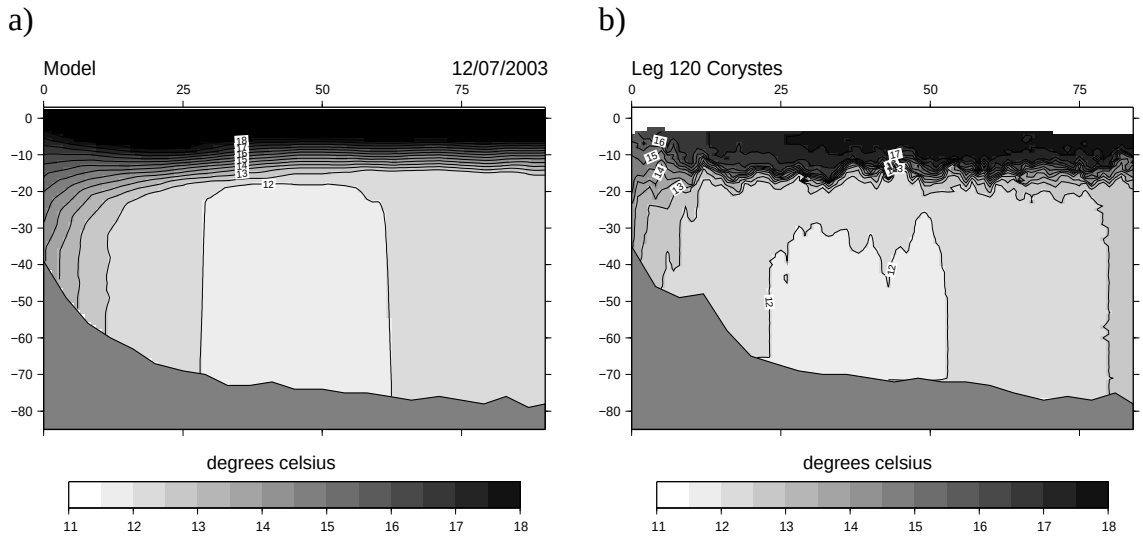

Fig. 6. Vertical pattern of temperature along leg 120 of the Corystes campaign computed by the model (a) and measured by the scanfish (b).

symbol	parameter	value	unit	source
Detrital matters				
$minN0_w$	N nimeralization rate at 0 ° C in water	0.025	d^{-1}	adjusted
$nit0_w$	nitrification rate at 0 ° C in water	0.023	d^{-1}	adjusted
$minP0_w$	P nimeralization rate at 0 ° C in water	0.02	d^{-1}	adjusted
$disSi0_w$	Si dissolution rate at 0 ° C in water	0.005	d^{-1}	Huret, 2005
$minN0_s$	N nimeralization rate at 0 ° C in sediment	0.01	d^{-1}	adjusted
$nit0_s$	nitrification rate at 0 ° C in sediment	0.02	d^{-1}	adjusted
$minP0_s$	P nimeralization rate at 0 ° C in sediment	0.01	d^{-1}	adjusted
$disSi0_s$	Si dissolution rate at 0 ° C in sediment	0.0035	d^{-1}	Cugier *et al.*, 2005b
$K_{O_2}^{min}$	half-saturation constant of O_2 in remin.	0.6	*adim.*	Cugier *et al.*, 2005b
$K_{O_2}^{nit}$	half-saturation constant of O_2 in nitrif.	1.2	*adim.*	Cugier *et al.*, 2005b
Particulate adsorbed phosphorus				
C_{adsop}	P adsorption rate	2.4	d^{-1}	Cugier *et al.*, 2005b
C_{desorp}	P desorption rate	0.12	$d^{-1}\ dm^3\ \mu mol^{-1}$	Cugier *et al.*, 2005b
Q_{adsop}^{max}	maximum P adsorption capacity	40	$\mu mol\ g^{-1}$	Cugier *et al.*, 2005b
Sedimentation processes and characteristics of the sediment				
w_{min}^{Dia}	diatom minimum sedimentation velocity	0.5	$m\ d^{-1}$	Loyer, 2001
w_{max}^{Dia}	diatom maximum sedimentation velocity	1.8	$m\ d^{-1}$	Loyer, 2001
w_{Zoo}^{det}	sedimentation velocity of zooplankton detritus	120	$m\ d^{-1}$	Huret, 2005
r_{Det}	radius of phytoplankton detritus	$1.5\ 10^{-5}$	m	Loyer, 2001
ρ_{Det}	density of phytoplankton detritus	2000	$kg\ m^{-3}$	Loyer, 2001
ν	molecular viscosity	10^{-6}	$m^2\ s^{-1}$	Loyer, 2001
w_{min}^{SPM}	SPM's minimum sedimentation velocity	$5\ 10^{-6}$	$m\ s^{-1}$	Cugier and Le Hir, 2000
w_{max}^{SPM}	SPM's maximum sedimentation velocity	10^{-5}	$m\ s^{-1}$	Cugier and Le Hir, 2000
τ_{cd}	threshold constraint for deposition	1.0	$N\ m^{-2}$	Cugier and Le Hir, 2000
τ_{ce}	threshold constraint for erosion	0.89	$N\ m^{-2}$	Cugier and Le Hir, 2000
c_{sed}	concentration of the sediment	500	$kg\ m^{-3}$	adjusted
er_{sed}	erosion rate	0.05	$kg\ m^{-2}\ s^{-1}$	Cugier and Le Hir, 2000

Table 5
Parameters used in mineralization processes and in exchanges of particles between water and sediment.

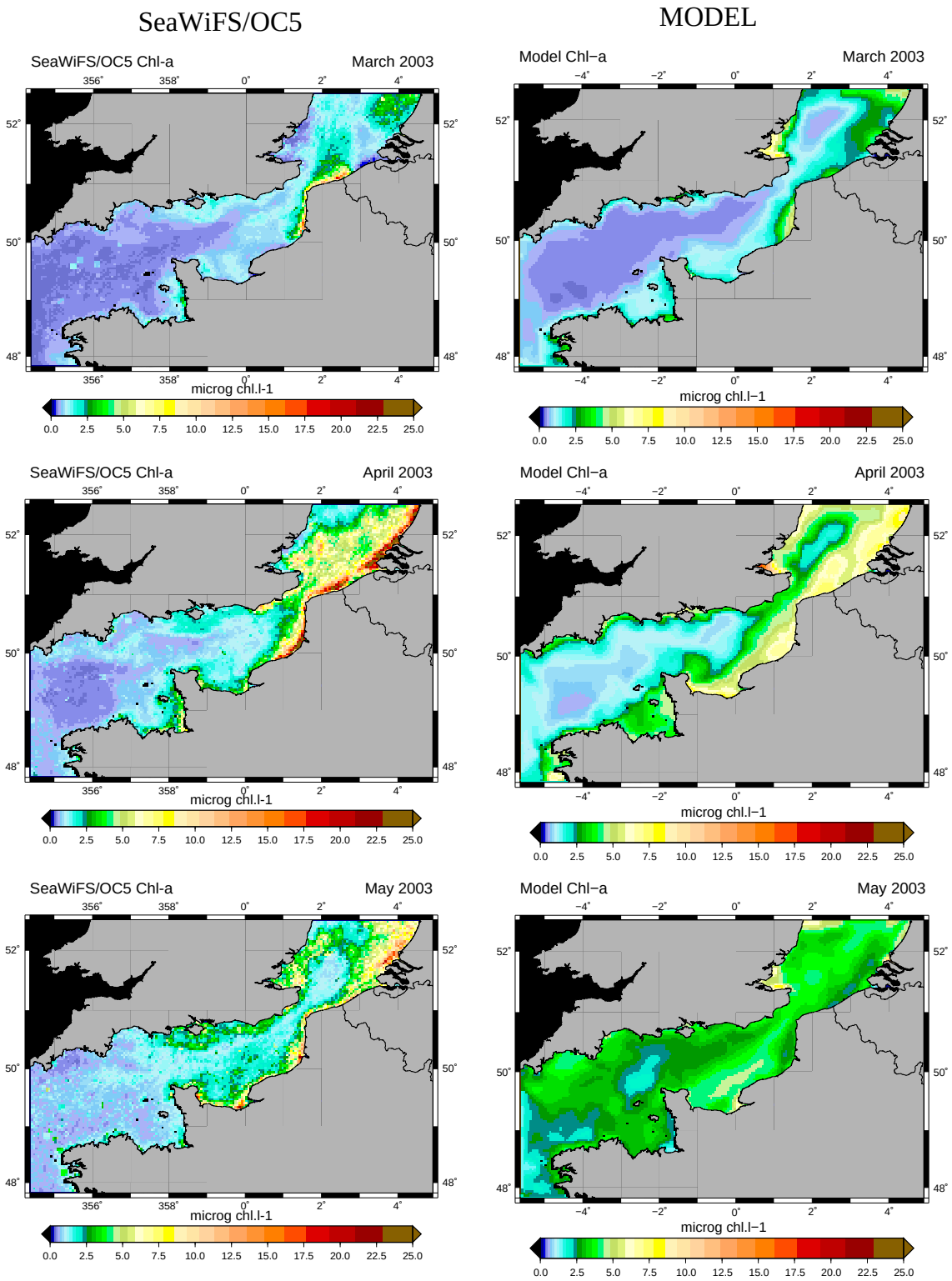

Fig. 7. Monthly mean of sea surface chlorophyll *a* situations calculated from SeaWiFS images (left) and outputs of the model (right).

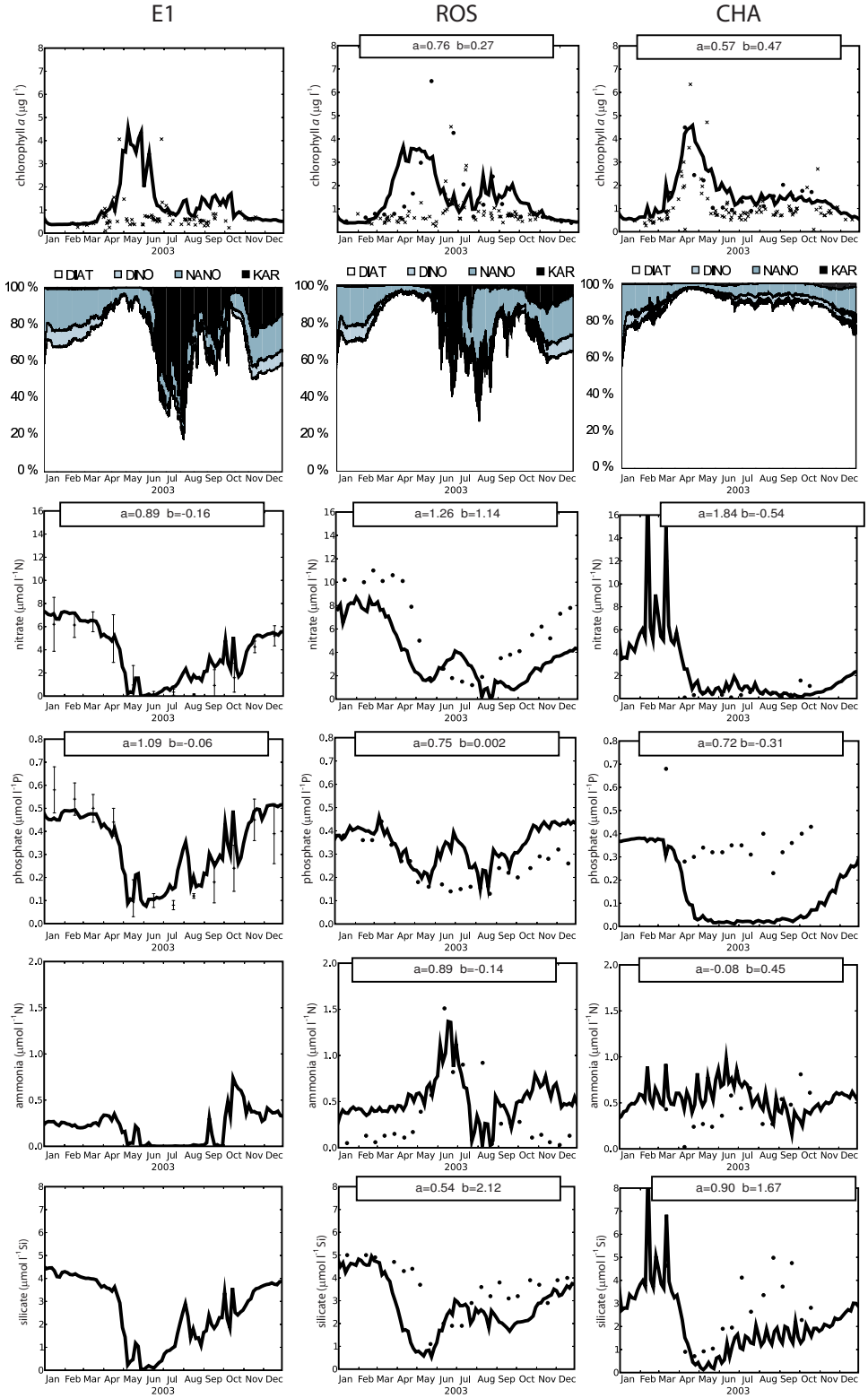

Fig. 8. 2003 annual cycle of nutrients, chlorophyll and phytoplanktonic successions for 3 stations. Results of the model (−), data from SeaWiFS (×) and *in situ* data (•). Nutrient data at Station E1 are monthly means from 1980-1987 data (Jordan and Joint, 1998).

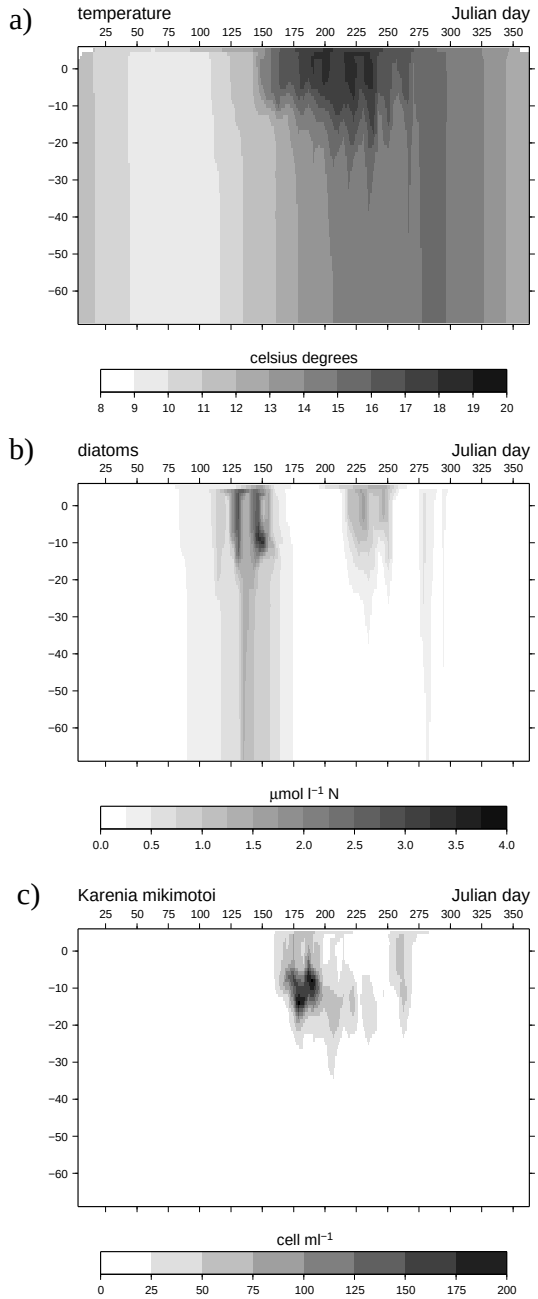

Fig. 9. Computed depth-time course of temperature (a), diatoms (b) and *Karenia mikimotoi* concentration (c) at Station 275 during 2003.

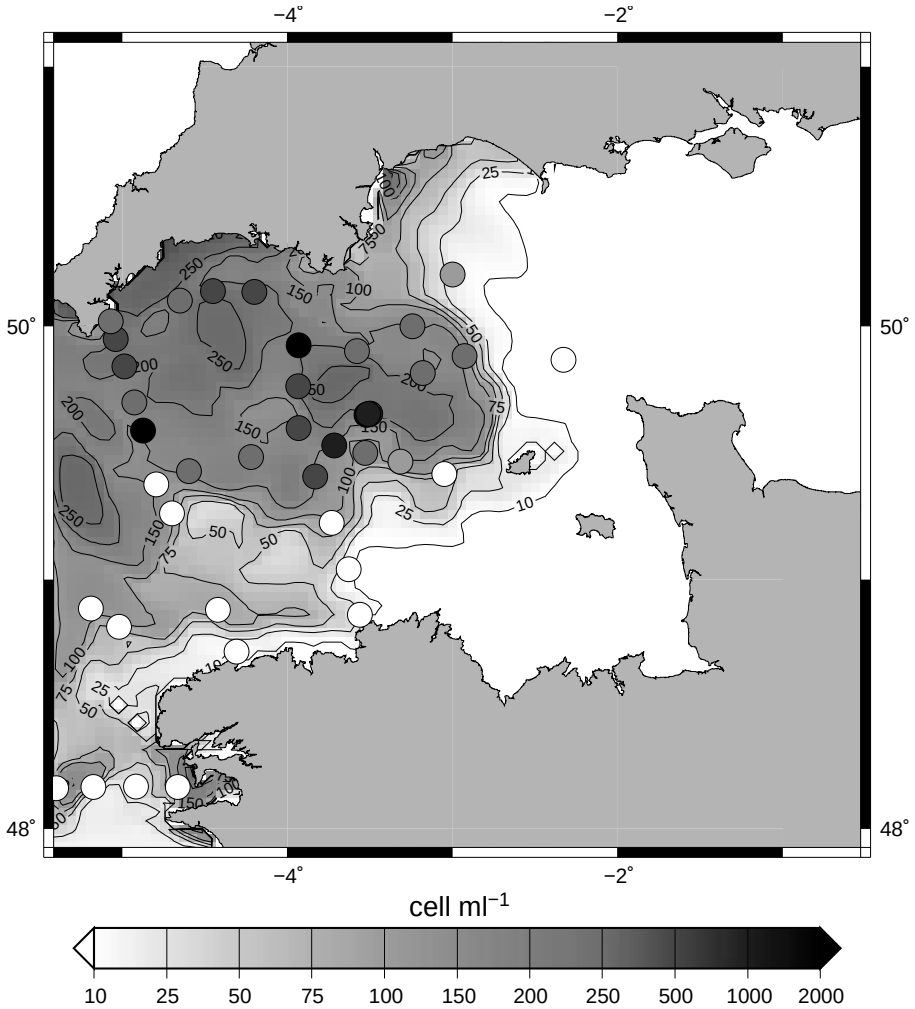

Fig. 10. Superimposition of depth maximum concentration of *Karenia mikimotoi* sampled during the Corystes Cruise (circles) and computed on the 14th July 2003.

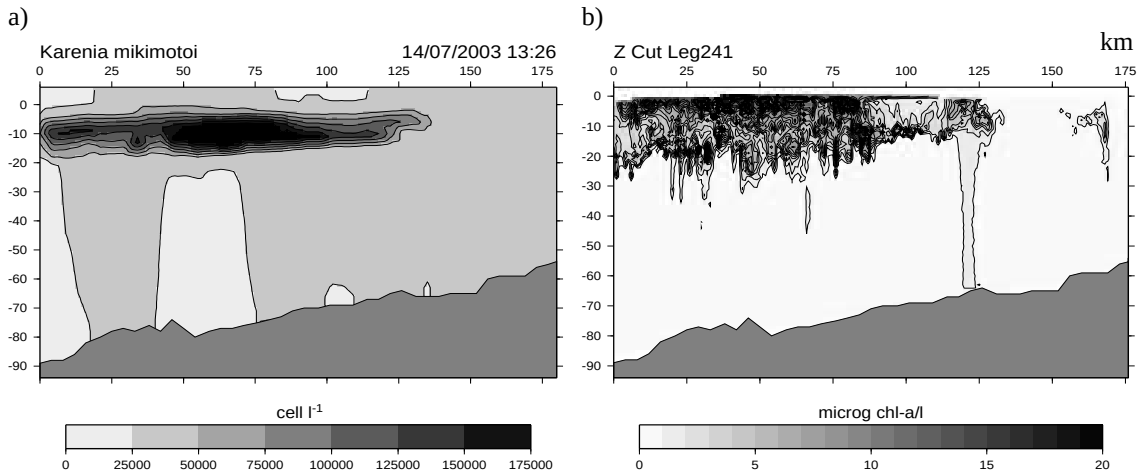

Fig. 11. Vertical pattern of the computed *Karenia mikimotoi* cell concentration (a) and mesured chlorophylle *a* concentration along scanfish section 241 (b).

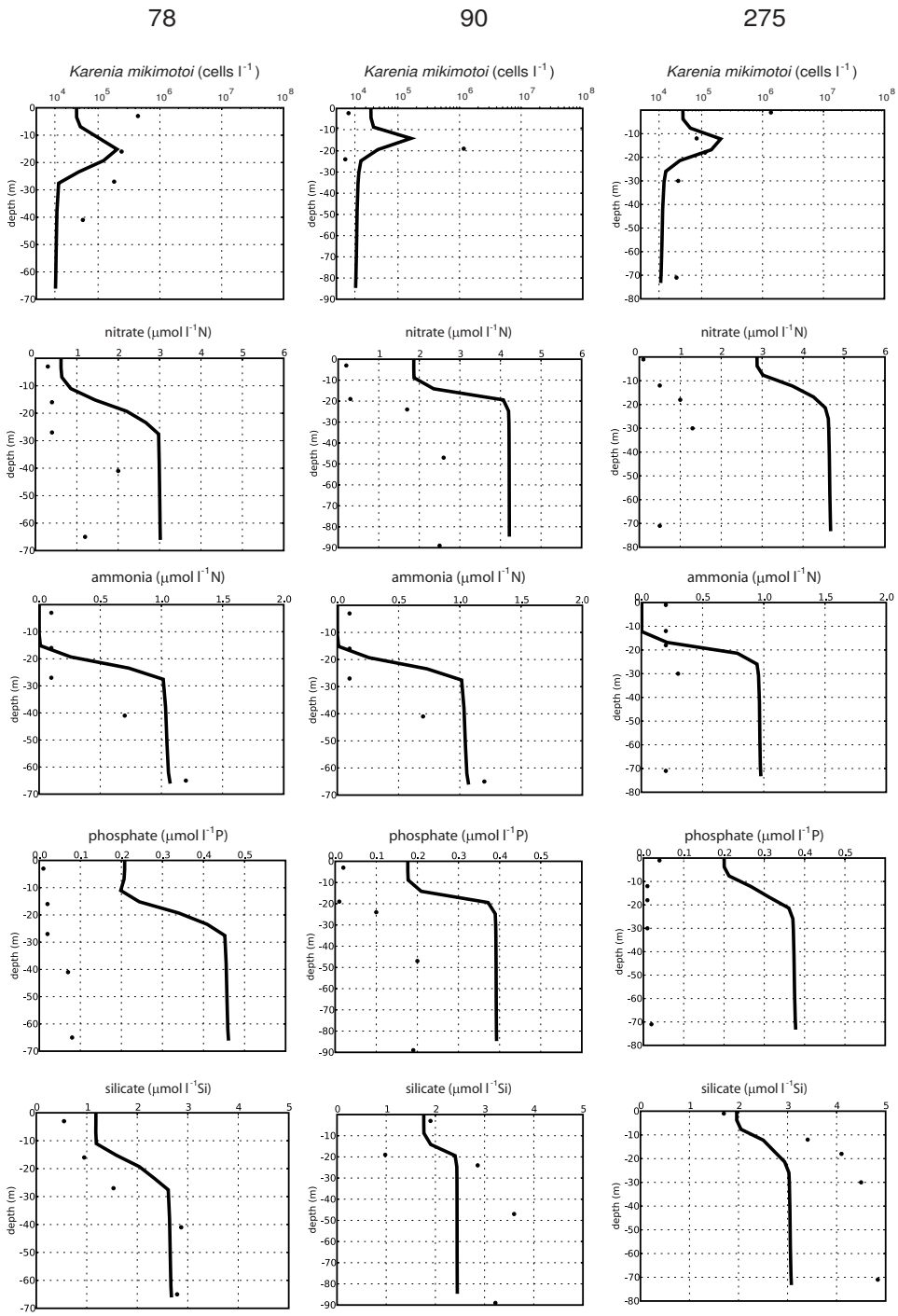

Fig. 12. Profiles of *Karenia mikimotoi* and nutrients from the Corystes Cruise (•) and model (−) at many stations located in Figure 2.

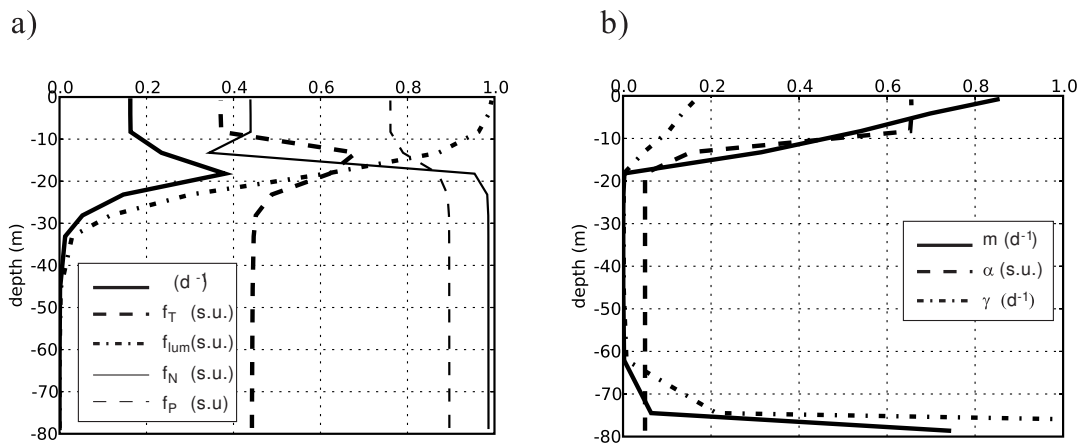

Fig. 13. Computed vertical distributions of growth limiting effects (a) and processes involved in the mortality of *Karenia mikimotoi* (b) at Station 70 (see Figure 2) the 12/th July 2003, at midday.

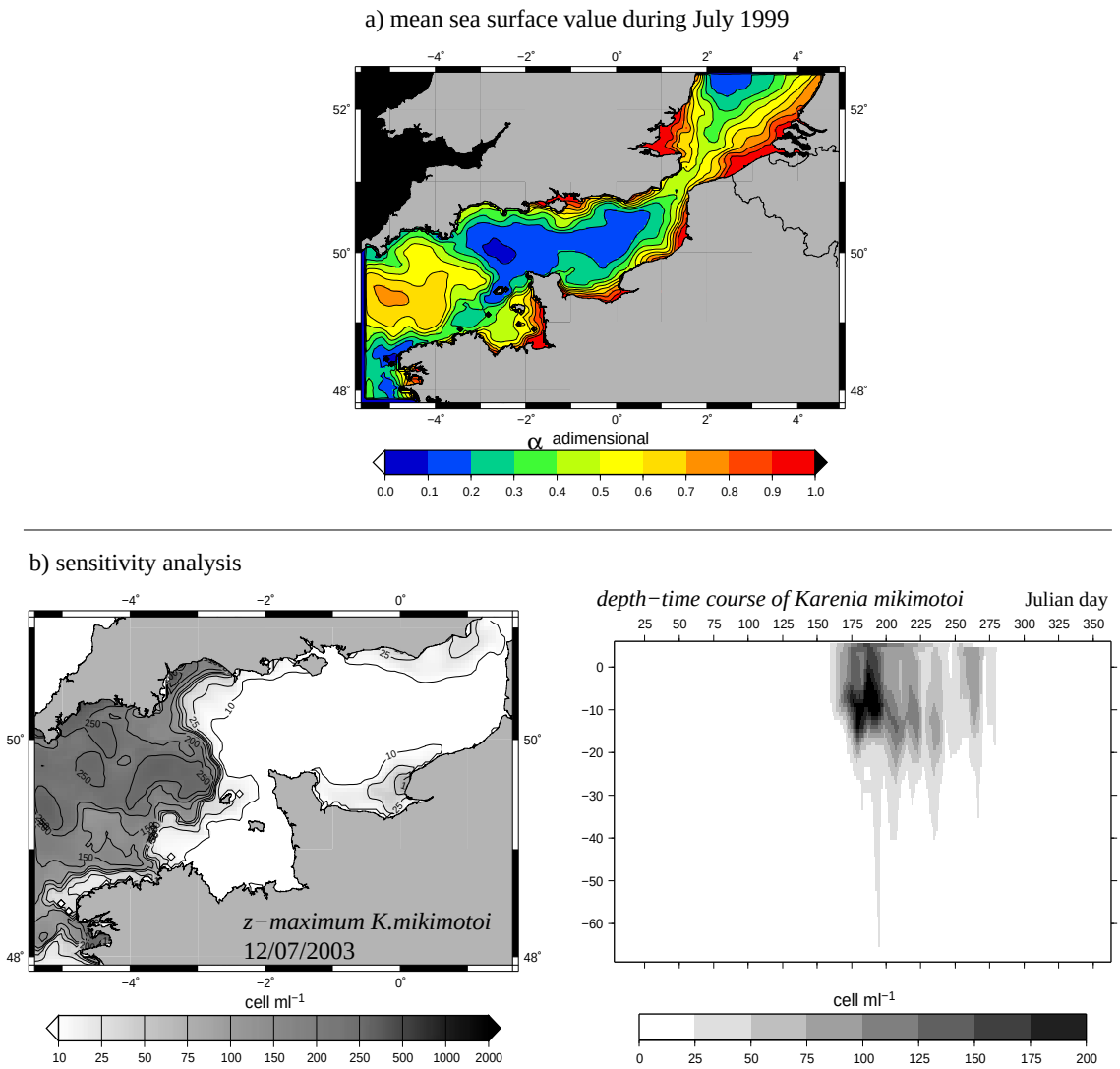

Fig. 14. Sensitivity analysis on the stickiness factor α. (a) Mean surface values of α in July 2003 during the nominal run. (b) Depth-maximum of *Karenia* the 12 th of July 2003 (left) and computed depth-time course of *Karenia* at Station 275 (right) during the special run when α is fixed ($\alpha = \alpha_{min}$).

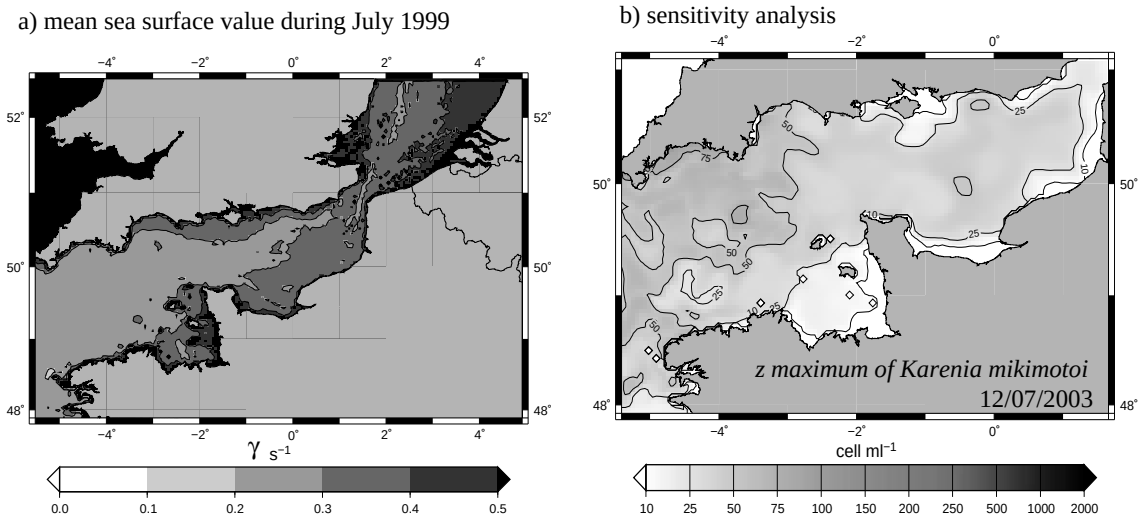

Fig. 15. Sensitivity analysis on the turbulent factor γ. (a) Mean surface values of the γ in April 2003 during the nominal run. (b) Depth-maximum of *Karenia* the 12 th of July 2003 of the special run when γ is fixed ($\gamma = 0.2\ s^{-1}$).

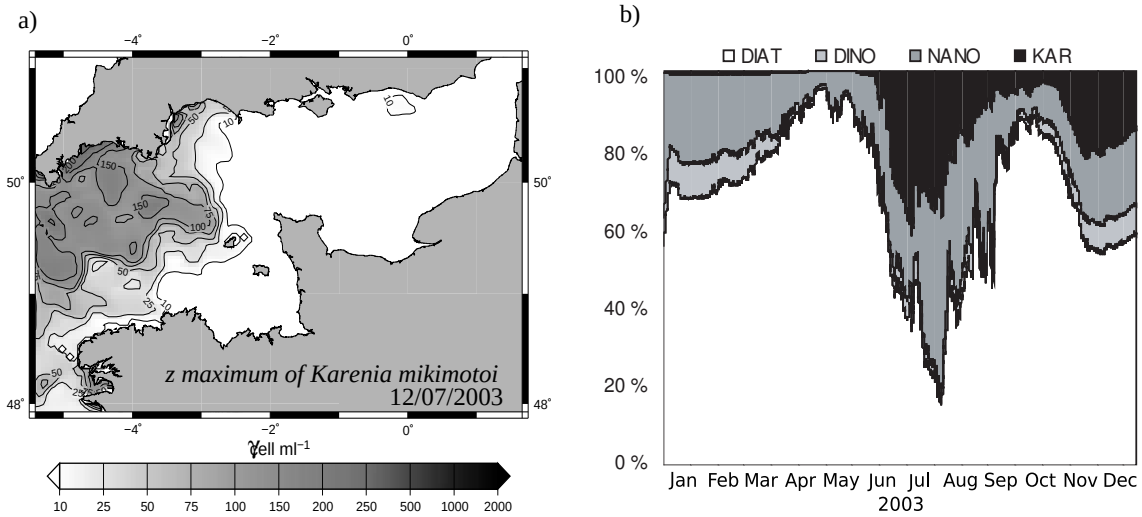

Fig. 16. The importance of the allelopathy. (a) Depth-maximum of *Karenia* the 12 th of July 2003 of the special run when $r_{all} = 0.$, (b) relative importance of phytoplanktonik groups at Station E1 when $r_{all} = 1$.

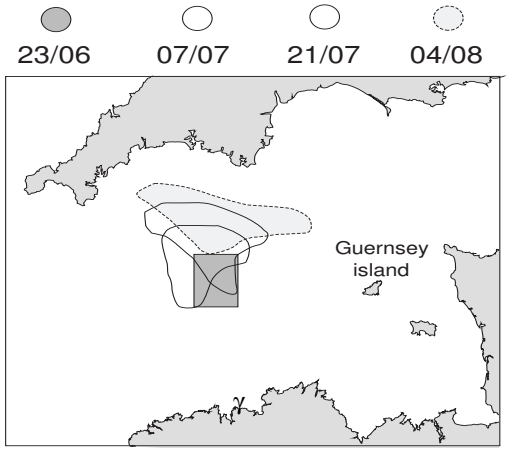

Fig. 17. Fate of a passive tracer spill during the *Karenia mikimotoi* bloom. Isolines of surface concentration > 10 indicated every week time lag.